

**TRANSITION FROM RESONANCES TO SURFACE WAVES IN  
 $\pi^+$ -p ELASTIC SCATTERING**

ENRICO DE MICHELI

*IBF – Consiglio Nazionale delle Ricerche  
Via De Marini, 6 - 16149 Genova, Italy*

GIOVANNI ALBERTO VIANO

*Dipartimento di Fisica – Università di Genova,  
Istituto Nazionale di Fisica Nucleare – Sezione di Genova,  
Via Dodecaneso, 33 - 16146 Genova, Italy*

ABSTRACT. In this article we study resonances and surface waves in  $\pi^+$ -p scattering. We focus on the sequence whose spin-parity values are given by  $J^P = \frac{3}{2}^+, \frac{7}{2}^+, \frac{11}{2}^+, \frac{15}{2}^+, \frac{19}{2}^+$ . A widely-held belief takes for granted that this sequence can be connected by a moving pole in the complex angular momentum (CAM) plane, which gives rise to a linear trajectory of the form  $J = \alpha_0 + \alpha' m^2$ ,  $\alpha' \sim 1/(\text{GeV})^2$ , which is the standard expression of the Regge pole trajectory. But the phenomenology shows that only the first few resonances lie on a trajectory of this type. For higher  $J^P$  this rule is violated and is substituted by the relation  $J \sim kR$ , where  $k$  is the pion-nucleon c.m.s. momentum, and  $R \sim 1$  fm. In this article we prove: (a) Starting from a non-relativistic model of the proton, regarded as composed by three quarks confined by harmonic potentials, we prove that the first three members of this  $\pi^+$ -p resonance sequence can be associated with a vibrational spectrum of the proton generated by an algebra  $\mathfrak{sp}(3, \mathbb{R})$ . Accordingly, these first three members of the sequence can be described by Regge poles and lie on a standard linear trajectory. (b) At higher energies the amplitudes are dominated by diffractive scattering, and the creeping waves play a dominant role. They can be described by a second class of poles, which can be called Sommerfeld's poles, and lie on a line nearly parallel to the imaginary axis of the CAM-plane. (c) The Sommerfeld pole which is closest to the real axis of the CAM-plane is dominant at large angles, and describes in a proper way the backward diffractive peak in both the following cases: at fixed  $k$ , as a function of the scattering angle, and at fixed scattering angle  $\theta = \pi$ , as a function of  $k$ . (d) The evolution of this pole, as a function of  $k$ , is given in first approximation by  $J \simeq kR$ .

---

*E-mail addresses:* enrico.demicheli@cnr.it, viano@ge.infn.it.

## 1. INTRODUCTION

At the end of their review paper on baryon spectroscopy, Hey and Kelly write [1]: “*The ideas of spin  $\frac{1}{2}$  quarks and a hidden color degree of freedom must surely rate as the most significant achievements of baryon spectroscopy. Another piece of current dogma, taking much support from the baryon spectrum, is the widely-held belief in linear Regge trajectories as a function of mass-squared*”. But, after a more careful phenomenological analysis, based, in particular, on the work of Hendry [2], they conclude: “*The conventional picture of linear Regge trajectories with universal slope is not well-established.*” Regarding the  $\pi^+$ -p collision, Hendry writes [3]: “*The first few resonances are consistent with a straight-line trajectory; however, as we increase the spins, the resonances appear to deviate from this trajectory.*”

In the conventional Regge-type phenomenology, the relationship between the total spin  $J$  and the squared-mass is given (with standard notation) by:  $J = \alpha_0 + \alpha' m^2$ , the slope of the trajectory being  $\alpha' \sim 1/(\text{GeV})^2$ .

Furthermore, it is often found in the literature the expression “rotational excitations” in view of the fact that states of the hadronic spectrum lying on the same trajectory possess the property  $\Delta J = 2$  [4, pag. 4][5]. In this connection several authors, notably Dothan, Gell-Mann, Ne’eman [6], Šijački [7], and Ne’eman [8], call the attention to the non-compact algebra of the  $\text{SL}(3, \mathbb{R})$  group which, on the other hand, plays a relevant role in describing the nuclear rotational motion [7]. Therefore, we can say that the scenario appears to be far from being neat and clear, nor it is changed significantly in more recent time.

In this article, instead of studying hadronic sequences in their wide generality, we focus only on the sequence of resonances obtained in the  $\pi^+$ -p elastic scattering, whose  $J^P$  values are given by:  $J^P = \frac{3}{2}^+, \frac{7}{2}^+, \frac{11}{2}^+, (\frac{15}{2}^+, \frac{19}{2}^+)$ . This is one of the most widely explored sequences in particle physics, and is generated by the interaction of a  $\pi^+$  meson with a proton: if the total angular momentum of the proton (composed of three quarks) is  $L = 0$ , then adding the angular momentum of the pion, which is  $1\hbar$  ( $\hbar = 1$ ), and the proton spin, we have  $J^P = \frac{3}{2}^+$ . If we consider also the isospin of the  $\pi^+$ -p system, we have the famous  $\Delta(\frac{3}{2}, \frac{3}{2})$  resonance, which can be regarded as the first member of a family of even parity resonances, which correspond to the following sequence of values of the angular momentum  $L$  of the proton:  $L = 0^+, 2^+, 4^+, (6^+, 8^+)$ . Here we prefer to distinguish and keep separated the last two members of the sequence, with  $J^P = \frac{15}{2}^+, \frac{19}{2}^+$ , in view of the considerations which we are going to develop below. In fact, as the phenomenological analysis of Hendry shows [2], the linear rising of the Regge trajectory in the  $\pi^+$ -p elastic scattering, is violated by the members of the family with high  $J$ , in particular, with  $J^P = \frac{15}{2}^+, \frac{19}{2}^+$ . One of the purposes of the present article is precisely to show that this phenomenon, in the specific case of  $\pi^+$ -p elastic scattering, corresponds to a transition from sharp resonances, which lie on a trajectory of standard form  $J = \alpha_0 + \alpha' m^2$  ( $\alpha' \sim 1/(\text{GeV})^2$ ), to surface waves. The resonances are properly described by Regge poles, and can be associated with a vibrational spectrum generated by the symplectic algebra  $\mathfrak{sp}(3, \mathbb{R})$ . Differently, surface waves are described by an other class of poles, which we call Sommerfeld poles, whose location and motion in the complex angular momentum (CAM) plane are radically different from those of the resonance poles.

The theory we present in Section 2 splits into two parts: in the first part we show that the resonances (in particular, the first three states with  $J^P = \frac{3}{2}^+, \frac{7}{2}^+, \frac{11}{2}^+$ ) lie on a linear trajectory which can be associated with a vibrational type spectrum. To this end we develop a non-relativistic quark model, studying the three-body dynamics generated by the quarks ( $uud$ ) confined by harmonic-type potentials. We are thus led to the SU(3) classification of three-particle states; in particular, by removing the degeneracies of the harmonic oscillator, we obtain an Elliott-type rotational spectrum [9]. But, it is easy to see that a trajectory of the form  $J = \alpha_0 + \alpha' m^2$  is far from being generated by a rotational spectrum, in spite of the rule  $\Delta J = 2$ . It rather appears to be closer related to a relativistic extension of a harmonic oscillator model, where  $L$  is proportional to the energy, i.e.,  $L \propto E$ . In fact, note that, accounting for the relativistic kinematics, one could expect to get  $L \propto E^2$ , which yields a behavior which corresponds to a Regge-type trajectory [10, pag. 91]. One is thus led to an enlargement of the spectrum generating group (SGG)  $SL(3, \mathbb{R})$  toward precisely the SGG  $Sp(3, \mathbb{R})$ . Accordingly we obtain a vibrational-like spectrum, associated with a symplectic group, which represents, *at the non-relativistic level*, a model of a linear trajectory.

In the elastic  $\pi^+$ -p collision the first few unstable states are sharp resonances (as a typical example keep in mind the  $\Delta(\frac{3}{2}, \frac{3}{2})$  resonance), where only one partial wave is neatly dominant. But, as the energy increases, inelastic and reaction channels open: the scenario changes drastically. The elastic unitarity condition does not hold anymore, and the target may be thought of as a ball totally or partially opaque at the center and with a semitransparent shell at the border. At these energies the colliding beam undergoes diffraction. The grazing trajectories hitting the target split into two rays: one ray leaves the target tangentially, while the other one propagates along the edge, creeping around the target. We have the surface wave phenomenon. Instead of a single dominant partial wave, this phenomenon is due to a packet of partial waves. Accordingly, the standard Fourier-Legendre expansion in partial waves of the scattering amplitude converges slowly, and it is therefore unsuited to describe surface waves. A Watson-type resummation of the partial wave expansion becomes needed, and can be performed as Sommerfeld did in connection with the diffraction of radio waves around the earth [11]. Following Sommerfeld, surface waves can still be described in terms of poles, but these poles manifest features and behavior rather different from those describing resonances, e.g., instead of being located close to the real axis in the CAM-plane, they lie on a line which is nearly parallel to the imaginary axis. Therefore, in order to distinguish clearly these two different classes of poles, we call *Regge poles* those referring to resonances, and *Sommerfeld poles* those referring to surface waves. The analysis leading to the Sommerfeld poles is developed in detail in Subsection 2.2.

In Section 3 we show that it is indeed the difference between these two classes of poles which explains the phenomenological results. More precisely, Section 3 is split into two parts: in the first part we study the first three resonances ( $J^P = \frac{3}{2}^+, \frac{7}{2}^+, \frac{11}{2}^+$ ), and show that they lie on a straight line trajectory of Regge type. The fits of the cross-sections are analyzed by means of poles in the CAM-plane, and results in agreement with the first part of the theory are then obtained. In the second part of Section 3 the cross-section is analyzed at higher energy, and we study in detail the effects of the surface waves with particular attention to the transition from resonances to creeping waves. Even in this case we obtain results which agree

with the second part of the theory. Finally, in Section 4 some conclusions are summarized.

## 2. THE THEORY

### 2.1. Spectrum of the resonances in $\pi^+$ -p elastic scattering.

2.1.1. *Non-relativistic Schrödinger dynamics of three bodies confined by harmonic potentials.* In the quark model the proton is composed by two quarks  $u$  and one quark  $d$ . The mass of these quarks is approximately equal, and therefore we may treat, with good approximation, these three bodies as having the same mass. The possible mathematical tools for tackling the problem are: the hyperspherical formalism [12], and the Faddeev equations [12]. Since the study of symmetries and, accordingly, the group theoretical methods, play in our analysis a very relevant role, the hyperspherical formalism appears more suitable to our purpose. The hyperspherical method has been used frequently, and is well-known [12]. Therefore, we run through this argument very rapidly, and we will give the necessary results in a form appropriate to our successive group theoretical analysis.

Let us consider three particles of equal mass  $m$ , whose positions are described by the vectors  $\mathbf{r}_k = (x_k, y_k, z_k)$ , ( $k = 1, 2, 3$ ). The kinetic energy operator reads

$$(1) \quad T = -\frac{1}{2m}(\Delta_1 + \Delta_2 + \Delta_3) \quad (\hbar = 1),$$

where  $\Delta_k = \partial^2/\partial x_k^2 + \partial^2/\partial y_k^2 + \partial^2/\partial z_k^2$  ( $k = 1, 2, 3$ ). We now introduce the Jacobi and center of mass coordinates, defined as follows:

$$(2a) \quad \boldsymbol{\xi}_1 = \frac{\mathbf{r}_1 - \mathbf{r}_2}{\sqrt{2}},$$

$$(2b) \quad \boldsymbol{\xi}_2 = \left(\frac{2}{3}\right)^{1/2} \left(\frac{\mathbf{r}_1 + \mathbf{r}_2}{2} - \mathbf{r}_3\right),$$

$$(2c) \quad \mathbf{R}_{\text{c.m.}} = \frac{\mathbf{r}_1 + \mathbf{r}_2 + \mathbf{r}_3}{3} \quad |\mathbf{r}_k| = \sqrt{x_k^2 + y_k^2 + z_k^2}.$$

The kinetic energy operator can be written in these coordinates as

$$(3) \quad T = -\frac{1}{2m} \left( \Delta_{\boldsymbol{\xi}_1} + \Delta_{\boldsymbol{\xi}_2} + \frac{1}{3} \Delta_{\mathbf{R}_{\text{c.m.}}} \right),$$

where

$$(4a) \quad \Delta_{\boldsymbol{\xi}_i} \equiv \frac{\partial^2}{[\partial(\boldsymbol{\xi}_i)_x]^2} + \frac{\partial^2}{[\partial(\boldsymbol{\xi}_i)_y]^2} + \frac{\partial^2}{[\partial(\boldsymbol{\xi}_i)_z]^2} \quad (i = 1, 2),$$

$$(4b) \quad \Delta_{\mathbf{R}_{\text{c.m.}}} \equiv \frac{\partial^2}{[\partial(\mathbf{R}_{\text{c.m.}})_x]^2} + \frac{\partial^2}{[\partial(\mathbf{R}_{\text{c.m.}})_y]^2} + \frac{\partial^2}{[\partial(\mathbf{R}_{\text{c.m.}})_z]^2},$$

$(\boldsymbol{\xi}_i)_x, (\boldsymbol{\xi}_i)_y, (\boldsymbol{\xi}_i)_z$  and  $(\mathbf{R}_{\text{c.m.}})_x, (\mathbf{R}_{\text{c.m.}})_y, (\mathbf{R}_{\text{c.m.}})_z$  denoting the  $x, y, z$  components of the vectors  $\boldsymbol{\xi}_i$  and  $\mathbf{R}_{\text{c.m.}}$ , respectively. Then, the kinetic energy of the center of mass can be separated from that of the relative motion  $T_R$ :

$$(5) \quad T_R = -\frac{1}{2m} (\Delta_{\boldsymbol{\xi}_1} + \Delta_{\boldsymbol{\xi}_2}).$$

Now, it is convenient to combine the vectors  $\boldsymbol{\xi}_1$  and  $\boldsymbol{\xi}_2$  into a single vector  $\boldsymbol{\Xi} = \begin{pmatrix} \boldsymbol{\xi}_1 \\ \boldsymbol{\xi}_2 \end{pmatrix}$ , whose Cartesian components will be denoted by  $\Xi_1, \Xi_2, \dots, \Xi_6$ . We can now consider a sphere embedded in  $\mathbb{R}^6$ , whose squared radius is  $\rho^2 = \boldsymbol{\xi}_1^2 + \boldsymbol{\xi}_2^2$  and,

accordingly, represent the components of  $\Xi$  in terms of the spherical coordinates  $(\rho, \theta_1, \dots, \theta_5)$  as follows:

$$(6) \quad \begin{aligned} \Xi_1 &= \rho \sin \theta_5 \sin \theta_4 \cdots \sin \theta_1, \\ \Xi_2 &= \rho \sin \theta_5 \sin \theta_4 \cdots \cos \theta_1, \\ &\dots\dots\dots \\ \Xi_5 &= \rho \sin \theta_5 \cos \theta_4, \\ \Xi_6 &= \rho \cos \theta_5. \end{aligned}$$

In terms of spherical coordinates the Laplace–Beltrami operator reads [13]

$$(7) \quad \begin{aligned} \Delta &= \frac{1}{\rho^5} \frac{\partial}{\partial \rho} \left( \rho^5 \frac{\partial}{\partial \rho} \right) + \frac{1}{\rho^2 \sin^4 \theta_5} \frac{\partial}{\partial \theta_5} \left( \sin^4 \theta_5 \frac{\partial}{\partial \theta_5} \right) \\ &+ \frac{1}{\rho^2 \sin^2 \theta_5 \sin^3 \theta_4} \frac{\partial}{\partial \theta_4} \left( \sin^3 \theta_4 \frac{\partial}{\partial \theta_4} \right) \\ &+ \cdots + \frac{1}{\rho^2 \sin^2 \theta_5 \sin^2 \theta_4 \cdots \sin^2 \theta_2} \frac{\partial^2}{\partial \theta_1^2}, \end{aligned}$$

and, by separating the radial part from the angular one, we have:

$$(8) \quad \Delta = \frac{1}{\rho^5} \frac{\partial}{\partial \rho} \left( \rho^5 \frac{\partial}{\partial \rho} \right) + \frac{1}{\rho^2} \Delta_0,$$

where  $\Delta_0$  is the Laplace–Beltrami operator acting on the unit sphere  $\mathbb{S}^5$  embedded in  $\mathbb{R}^6$  [13].

Let us now introduce the harmonic polynomials of degree  $j$ , which may be written as  $\rho^j \Theta_j(\theta_1, \dots, \theta_5)$  [13]. Then, from (8) we obtain

$$(9) \quad \begin{aligned} \Delta [\rho^j \Theta_j(\theta_1, \dots, \theta_5)] \\ = j(j+4)\rho^{(j-2)} \Theta_j(\theta_1, \dots, \theta_5) + \rho^{(j-2)} \Delta_0 \Theta_j(\theta_1, \dots, \theta_5) = 0, \end{aligned}$$

which gives

$$(10) \quad \Delta_0 \Theta_j(\theta_1, \dots, \theta_5) = -j(j+4) \Theta_j(\theta_1, \dots, \theta_5).$$

Next, we introduce a potential of the following form:

$$(11) \quad V(\rho) = G [|\mathbf{r}_1 - \mathbf{r}_2|^2 + |\mathbf{r}_1 - \mathbf{r}_3|^2 + |\mathbf{r}_2 - \mathbf{r}_3|^2] = 3G\rho^2,$$

which is a *confining potential of harmonic type*.

The Schrödinger equation reads:

$$(12) \quad H\psi = \left( -\frac{1}{2m} \Delta + V \right) \psi = E\psi,$$

where  $E$  denotes the energy, and the operator  $\Delta$  and the potential  $V$  are defined by formulae (7) and (11), respectively. Next, by separating in the wavefunction  $\psi(\rho; \theta_1, \dots, \theta_5)$  the radial variable from the angular ones, we have the following equations:

$$(13) \quad \frac{1}{\rho^5} \frac{d}{d\rho} \left( \rho^5 \frac{dR_j}{d\rho} \right) - \frac{j(j+4)}{\rho^2} R_j + 2m[E - V(\rho)]R_j = 0,$$

$$(14) \quad \Delta_0 \Theta_j(\theta_1, \dots, \theta_5) = -j(j+4) \Theta_j(\theta_1, \dots, \theta_5),$$

The solutions of Eq. (13) are:

$$(15) \quad R_j(\rho) = \rho^j \exp\left(-\frac{1}{2}\sigma^2\rho^2\right), \quad \sigma = (mK)^{1/4},$$

$$(16) \quad E_j = (j+3)\omega, \quad \omega = \sqrt{\frac{K}{m}},$$

where  $K = 6G$ .

**Remark 1.** It is worth noting that the zero-point energy in the harmonic spectrum in (16) is:  $E_0 = 3\omega$  ( $\hbar = 1$ ),  $\omega = \sqrt{K/m}$ ,  $K = 6G$ ,  $G = V(\rho)/(3\rho^2)$ , and it is therefore strictly related to the strength of the confining potential.

Analogously to what done for the coordinates of the particles, we introduce for the momenta the vector  $\mathbf{\Gamma} = \begin{pmatrix} \mathbf{p}_{\xi_1} \\ \mathbf{p}_{\xi_2} \end{pmatrix}$ , where

$$(17a) \quad \mathbf{p}_{\xi_1} = \frac{\mathbf{q}_1 - \mathbf{q}_2}{\sqrt{2}},$$

$$(17b) \quad \mathbf{p}_{\xi_2} = \left(\frac{2}{3}\right)^{1/2} \left(\frac{\mathbf{q}_1 + \mathbf{q}_2}{2} - \mathbf{q}_3\right),$$

$$(17c) \quad \mathbf{p}_{\mathbf{R}_{c.m.}} = \frac{\mathbf{q}_1 + \mathbf{q}_2 + \mathbf{q}_3}{3},$$

and  $\mathbf{q}_k = m\dot{\mathbf{r}}_k$  ( $\dot{\mathbf{r}}_k = d\mathbf{r}_k/dt$ ;  $k = 1, 2, 3$ ) are the momenta of the particles. Next, we define the *grand-angular-momentum-tensor* [14], which is an antisymmetric  $6 \times 6$  tensor whose elements are

$$(18) \quad \Lambda_{kl} = \Xi_k \Gamma_l - \Xi_l \Gamma_k \quad (k, l = 1, 2, \dots, 6).$$

Now, we associate to the momentum  $\mathbf{\Gamma}$  the following differential operators:

$$(19) \quad \Gamma_k = -i\frac{\partial}{\partial \Xi_k} \quad (\hbar = 1; k = 1, 2, \dots, 6).$$

Then the following commutation rules hold true:

$$(20) \quad [\Xi_k, \Gamma_l] = i\delta_{kl} \quad (k, l = 1, 2, \dots, 6).$$

Substituting (19) into (18), we have

$$(21) \quad \Lambda_{kl} = -i \left( \Xi_k \frac{\partial}{\partial \Xi_l} - \Xi_l \frac{\partial}{\partial \Xi_k} \right) \quad (k, l = 1, 2, \dots, 6),$$

and the following commutation rules [14]:

$$(22a) \quad [\Lambda_{kl}, \Lambda_{mn}] = 0 \quad k \neq l \neq m \neq n$$

$$(22b) \quad [\Lambda_{kl}, \Lambda_{lm}] = -i\Lambda_{km}$$

$$(22c) \quad \Lambda_{kl} = -\Lambda_{lk}.$$

We can now introduce the quantity

$$(23) \quad \Lambda^2 = \frac{1}{2} \sum_{k,l=1}^6 \Lambda_{kl}^2,$$

which satisfies the following commutation rules:

$$(24) \quad [\Lambda^2, \Lambda_{kl}] = 0 \quad (k, l = 1, 2, \dots, 6).$$

Finally, rewriting  $\Lambda^2$  in terms of spherical coordinates, and in view of (14), we obtain

$$(25) \quad \Lambda^2 \Theta_j = -\Delta_0 \Theta_j = j(j+4) \Theta_j.$$

2.1.2. *Permutation group on three objects and classification of three-particle states according to SU(3): rotational bands.* The three-body motion may be described by means of the relative position vector between the particles 1 and 2, and of the vector connecting the particle 3 with the center of mass of the pair 1–2, i.e., using the Jacobi coordinates, if and only if we can treat all three particles *symmetrically*.

The group  $S_3$  of permutations on three objects embraces six elements: the three transpositions  $P_{ik}$  (or interchange of particles  $i$  and  $k$ ,  $i < k$ ), and the three cyclic permutations:  $C = P_{23}P_{12}$ , which performs the transformation  $123 \rightarrow 312$ ,  $C^2$  whose effect is  $123 \rightarrow 231$ , and, finally,  $C^3 = e$ , i.e., the identity  $123 \rightarrow 123$ . The transpositions  $P_{ik}$  have matrix representation with determinant equal to  $-1$ , whereas the cyclic permutations have determinant equal to  $+1$ . Therefore the elements of  $S_3$  may be split into two classes, depending on the sign of their determinant. Moreover, the cyclic permutations enjoy a continuous connection to the identity, which lies entirely within the group  $S_3$  [15].

It is easy to see that the transformation of permutation takes us out of the space of the components of  $\xi_1$  alone or of  $\xi_2$  alone, and mix the two sets of components [15]. But  $\rho^2 = \xi_1^2 + \xi_2^2$  is an invariant under both three-dimensional rotations and permutations, and, in general, under all six-dimensional rotations [15]. Then a remarkable fact is that the elements of the permutation group yield to rotations in  $\mathbb{R}^6$ . *We are thus led to consider groups which act transitively on the sphere  $\mathbb{S}^5$  embedded in  $\mathbb{R}^6$ .* The first obvious choice in this direction is to consider the group  $SO(6)$ :  $\mathbb{S}^5$  can be regarded as the space  $SO(6)/SO(5)$  indeed. Consider now the Lie algebra  $\mathfrak{so}(6)$  associated with the group  $SO(6)$ . As well-known, the Lie algebra  $\mathfrak{g}$  of the group  $G$  can be identified with the tangent space to  $G$  at the identity element, i.e.,  $\mathfrak{g} \simeq T G|_e$ . In particular,  $\mathfrak{so}(6)$  is the Lie algebra consisting of all  $6 \times 6$  real skew-symmetric matrices, and is the real form of the complex Lie algebra  $D_3$  of dimension 15 (recall that the dimension of  $D_n$  is given by  $n(2n-1)$  [16]). But in Ref. [14] Dragt has proved that *not all* the elements of  $\mathfrak{so}(6)$  treat all three particles equivalently. This forces us to look for a subset of  $\mathfrak{so}(6)$  whose elements satisfy the fundamental requirement of treating all three particles equivalently. On the other hand, exponentiating this subalgebra, we must obtain a subgroup of  $SO(6)$ , which acts transitively on  $\mathbb{S}^5$ . *We have only one candidate which satisfies this condition, the group  $SU(3)$ .* In fact the space  $\mathbb{C}^n$  may be identified with the space  $\mathbb{R}^{2n}$ , by writing out in a fixed order real and imaginary parts of the vector components in  $\mathbb{C}^n$ . Therefore,  $\mathbb{S}^5$  may also be regarded as the unit sphere embedded in  $\mathbb{C}^3$ , and, accordingly, may be identified with the quotient space  $SU(3)/SU(2)$ :  $SU(3)$  acts transitively on  $\mathbb{S}^5$ , indeed. The Lie algebra  $\mathfrak{su}(3)$ , associated with the group  $SU(3)$ , consists of all  $3 \times 3$  skew-hermitian matrices  $Z$  with  $\text{Tr} Z = 0$ . It is one of the real forms of the complex Lie algebra  $A_2$ , whose dimension is 8 (recall that the dimension of  $A_n$  is  $n(n+2)$  [16]).

**Remark 2.** It is interesting to note that the Lie algebras  $\mathfrak{su}(3)$  and  $\mathfrak{sl}(3, \mathbb{R})$  are real forms of the same algebra  $A_2$  [17]. This fact is particularly relevant in connection with the analysis which will be developed in the next subsection.

On the other hand Dragt [14] introduces a subset of  $\mathfrak{so}(6)$  (i.e., a Lie algebra which he denotes  $L_1$ ) defined as the set of all elements  $F \in \mathfrak{so}(6)$  which commute with the cyclic permutation  $C = P_{23}P_{12}$ , that is, satisfying  $[C, F] = 0$ . Dragt proves that all the elements of  $L_1$  treat all three particles with complete symmetry: if one permutes the particles,  $L_1$  either remains unaffected or undergoes a sign change. Even in this latter case it is still impossible to tell which pair of particles has been interchanged, and which particle has been left alone [14]. The algebra  $L_1$  is nine-dimensional and isomorphic to the Lie algebra associated with the  $U(3)$  group. The operators of this algebra may be expressed either in Cartesian form or in spherical tensor form. If this latter form is used, then a scalar form can be separated from the remaining components, and these latter components form a Lie algebra  $L_2$  of dimension 8 isomorphic to the Lie algebra  $\mathfrak{su}(3)$ . *We can thus conclude that the three-particle states can be completely classified by their transformation properties according to the  $SU(3)$  group.*

This fact leads us to consider the sphere  $S^5$  as the unit sphere embedded in  $\mathbb{C}^3$ , identified with the space  $SU(3)/SU(2)$ ; accordingly, we define the complex vectors

$$(26a) \quad \mathbf{Z} = \boldsymbol{\xi}_1 + i\boldsymbol{\xi}_2, \quad \mathbf{Z}^* = \boldsymbol{\xi}_1 - i\boldsymbol{\xi}_2,$$

$$(26b) \quad \boldsymbol{\Pi} = \mathbf{p}_{\boldsymbol{\xi}_1} + i\mathbf{p}_{\boldsymbol{\xi}_2}, \quad \boldsymbol{\Pi}^* = \mathbf{p}_{\boldsymbol{\xi}_1} - i\mathbf{p}_{\boldsymbol{\xi}_2}.$$

Then we have

$$(27a) \quad \mathbf{Z} \cdot \mathbf{Z}^* = \boldsymbol{\xi}_1^2 + \boldsymbol{\xi}_2^2 = \rho^2,$$

$$(27b) \quad \boldsymbol{\Pi} \cdot \boldsymbol{\Pi}^* = \mathbf{p}_{\boldsymbol{\xi}_1}^2 + \mathbf{p}_{\boldsymbol{\xi}_2}^2 = -\Delta.$$

Next, setting in Eqs. (15) and (16)  $m = \hbar = 1$ ,  $G = 1/6$  ( $K = 1$ ), the total Hamiltonian can be written in the following form (see Eq. (12)):

$$(28) \quad H = -\frac{1}{2}\Delta + V = \frac{1}{2}(\boldsymbol{\Pi} \cdot \boldsymbol{\Pi}^* + \mathbf{Z} \cdot \mathbf{Z}^*).$$

In order to deal with the harmonic oscillator problem in the Fock space, we introduce the vector creation and annihilation operators [14]

$$(29a) \quad \mathbf{A}^\dagger = \frac{1}{\sqrt{2}}(\boldsymbol{\xi}_1 - i\mathbf{p}_{\boldsymbol{\xi}_1}), \quad \mathbf{A} = \frac{1}{\sqrt{2}}(\boldsymbol{\xi}_1 + i\mathbf{p}_{\boldsymbol{\xi}_1}),$$

$$(29b) \quad \mathbf{B}^\dagger = \frac{1}{\sqrt{2}}(\boldsymbol{\xi}_2 - i\mathbf{p}_{\boldsymbol{\xi}_2}), \quad \mathbf{B} = \frac{1}{\sqrt{2}}(\boldsymbol{\xi}_2 + i\mathbf{p}_{\boldsymbol{\xi}_2}),$$

which satisfy the following commutation rules:

$$(30a) \quad [A_k, A_l^\dagger] = \delta_{kl} \quad (k, l = 1, 2, 3),$$

$$(30b) \quad [B_k, B_l^\dagger] = \delta_{kl}.$$

Therefore, the Hamiltonian may be written in terms of creation and annihilation operators as

$$(31) \quad H = \frac{1}{2}(\mathbf{A}^\dagger \cdot \mathbf{A} + \mathbf{A} \cdot \mathbf{A}^\dagger + \mathbf{B}^\dagger \cdot \mathbf{B} + \mathbf{B} \cdot \mathbf{B}^\dagger).$$

Thanks to the commutation rules (30) we have

$$(32) \quad \mathbf{A} \cdot \mathbf{A}^\dagger = 3 + \mathbf{A}^\dagger \cdot \mathbf{A}, \quad \mathbf{B} \cdot \mathbf{B}^\dagger = 3 + \mathbf{B}^\dagger \cdot \mathbf{B},$$

and, therefore, we obtain

$$(33) \quad H = (\mathbf{A}^\dagger \cdot \mathbf{A} + \mathbf{B}^\dagger \cdot \mathbf{B} + 3) = N_A + N_B + 3,$$



where  $N_A$  and  $N_B$  are the occupation numbers associated with the operators  $\mathbf{A}^\dagger \cdot \mathbf{A}$  and  $\mathbf{B}^\dagger \cdot \mathbf{B}$ , respectively. Then, for the ground state  $|0\rangle$ , which is characterized by the conditions  $\mathbf{A}|0\rangle = \mathbf{B}|0\rangle = 0$ , we have  $H|0\rangle = 3|0\rangle$ , which represents the zero-point energy; correspondingly, the wavefunction is  $\exp(-\rho^2/2)$ .

Now, let  $j_1$  and  $j_2$  denote the eigenvalues of  $N_A$  and  $N_B$ , respectively. Then from Eqs. (16) and (33) we have  $j = j_1 + j_2$ .

For any group  $G$  of linear transformations in a  $n$ -dimensional space, the tensors of rank  $r$  form a vector space of  $n^r$  dimensions and constitute the basis for a representation of the group  $G$  [18]. By using permutation operators (Young symmetrizers), this representation can be decomposed into irreducible representations of  $G$ . Thus the whole space of the  $r^{\text{th}}$  rank tensors is reducible into subspaces consisting of tensors of different symmetry. In the case of  $\text{GL}(3)$ , the tableaux for tensors of rank  $r$  can contain at most three rows of length  $f_1, f_2, f_3$  with  $\sum f_i = r$ , and  $f_1 \geq f_2 \geq f_3 \geq 0$ . Consequently, an irreducible representation of  $\text{GL}(3)$  is characterized by the partition  $(f_1, f_2, f_3)$ . Next, it can be shown that  $(f_1, f_2, f_3)$  also serves as a label for irreducible representations of  $\text{U}(3)$  [14].

In general an irreducible representation of a group  $G$ , although being obviously a representation of any subgroup  $H$  of  $G$ , will not be irreducible with respect to  $H$ . However, in the reduction of  $\text{U}(n)$  to  $\text{SU}(n)$  (in particular of  $\text{U}(3)$  to  $\text{SU}(3)$ ) the irreducible representations of  $\text{U}(n)$  remain irreducible under  $\text{SU}(n)$  [9, 18]. A simplification does occur nevertheless in that certain representations which were inequivalent under  $\text{U}(n)$  become equivalent under  $\text{SU}(n)$  in view of the fact that  $\text{SU}(n)$  is a unimodular subgroup of  $\text{U}(n)$  [9]. Consequently, for  $\text{SU}(3)$  the partition  $(f_1, f_2, f_3)$  can be replaced by the differences:  $k_1 = f_1 - f_3$ ,  $k_2 = f_2 - f_3$ . Accordingly, the group  $\text{SU}(3)$  needs two rows to label its representations. Putting  $k_1 = j_1 + j_2$  and  $k_2 = j_1$  (i.e.,  $j_2 = k_1 - k_2$ ), we have the following Young pattern:



which corresponds to the representation  $(j_1, j_2)$ . Coming back to the three-body dynamics, we now introduce the total angular momentum  $\mathbf{L}$  about the center of mass [14], i.e.,

$$(34) \quad \mathbf{L} = \mathbf{r}_1 \times \mathbf{q}_1 + \mathbf{r}_2 \times \mathbf{q}_2 + \mathbf{r}_3 \times \mathbf{q}_3 - \mathbf{R}_{\text{c.m.}} \times \mathbf{p}_{\text{R}_{\text{c.m.}}}.$$

Note that  $\mathbf{R}_{\text{c.m.}}$  and  $\mathbf{p}_{\text{R}_{\text{c.m.}}}$  cannot vanish simultaneously since they do not commute. In the center of mass we have  $\mathbf{R}_{\text{c.m.}} = 0$ , while in the center of momentum frame we have  $\mathbf{p}_{\text{R}_{\text{c.m.}}} = 0$ . It follows from (34) that  $\mathbf{L}$  may be interpreted either as the total angular momentum about the center of mass or as the total angular momentum in the center of momentum frame. Finally, it is important to remark that  $\mathbf{L}$  involves the three particles equivalently. We are thus led to the following problem.

**Problem 1.** Determine the  $L$ -values,  $L(L+1)$  being the eigenvalues of  $\mathbf{L}^2$ , contained in the representation  $(j_1, j_2)$  of  $\text{SU}(3)$ .

This problem can be rephrased as follows: determine what irreducible representations of the group  $\text{SO}(3)$ , which are labelled by  $L$ , occur in an irreducible representation of the group  $\text{SU}(3)$ . Weyl [9, 19] has given a simple formula for the

dimension of a representation of  $U(n)$ , i.e.,

$$(35) \quad \dim(f_1, f_2, \dots, f_n) = \prod_{1 \leq i < k \leq n} \left( \frac{f_i - f_k + k - i}{k - i} \right).$$

Now,  $(2L + 1)$  is the dimension of the representation  $D_L$  of the rotation group. Then, Problem 1 is solved by the equality

$$(36) \quad \prod_{1 \leq i < k \leq 3} \left( \frac{f_i - f_k + k - i}{k - i} \right) = \sum_L \mu_L (2L + 1),$$

where  $\mu_L$  gives the number of times the representation  $D_L$  occurs in a certain representation of  $SU(3)$ . Equality (36) has been obtained by equating the characters of the representations in the specific case of the unit element: recall, indeed, that the character of a representation, corresponding to the unit element, gives the dimension of the representation. In the present case we have  $j_1 = k_2 = f_2 - f_3$ , and  $j_2 = k_1 - k_2 = f_1 - f_2$ . Therefore, from formula (36) it follows

$$(37) \quad (j_1 + 1)(j_2 + 1) \left( \frac{j_1 + j_2 + 2}{2} \right) = \sum_L \mu_L (2L + 1).$$

Since the l.h.s. of (37) is symmetric in  $j_1$  and  $j_2$ , it follows that  $\dim(j_1, j_2) = \dim(j_2, j_1)$ . Now, we consider two cases:

(a) Let  $j_1 = 2n$  ( $n$  integer) and  $j_2 = 0$ ; then

$$(38) \quad \begin{aligned} \dim(j_1, j_2) &= \dim(2n, 0) \\ &= (n + 1)(2n + 1) = \dim(D_0 + D_2 + \dots + D_{2n}). \end{aligned}$$

This means that the  $L$ -values that occur in the representation  $(2n, 0)$  are  $L = 0, 2, 4, \dots, 2n$  ( $\mu_L = 1$ ). We have thus obtained a *rotational* band of even parity.

(b) Let  $j_1 = 2n + 1$  ( $n$  integer) and  $j_2 = 0$ ; then

$$(39) \quad \begin{aligned} \dim(j_1, j_2) &= \dim(2n + 1, 0) \\ &= (n + 1)(2n + 3) = \dim(D_1 + D_3 + \dots + D_{2n+1}). \end{aligned}$$

This means that the  $L$ -values that occur in the representation  $(2n + 1, 0)$  are  $L = 1, 3, 5, \dots, 2n + 1$  ( $\mu_L = 1$ ). We have thus obtained a *rotational* band of odd parity.

Let us observe that levels with different values of  $L$ , but with the same value of  $j = j_1 + j_2$ , are degenerate. In order to remove these degeneracies one can first construct the Casimir operator  $C$  of the  $SU(3)$  group. Recall that this operator is a scalar under the group. In our case there are only two scalars, which one can form: one is the product  $(\mathbf{L} \cdot \mathbf{L})$  (where  $\mathbf{L}$  is the total angular momentum (34)); the second is the tensorial product  $(\mathbf{K} \otimes \mathbf{K})$ , where  $\mathbf{K}$  is a symmetric tensor which, in dyad notation, reads [14]:

$$(40) \quad \mathbf{K} = \frac{1}{\sqrt{3}} [(\mathbf{r}_1 - \mathbf{r}_2)\mathbf{q}_3 + (\mathbf{r}_2 - \mathbf{r}_3)\mathbf{q}_1 + (\mathbf{r}_3 - \mathbf{r}_1)\mathbf{q}_2 + \text{transpose}].$$

Note that  $\mathbf{K}$  involves the three particles equivalently [14]. The Casimir operator is that combination of these two products which also commutes with the group operators. Next one adds to the harmonic oscillator Hamiltonian a term proportional to the Casimir operator  $C$ . This latter will be diagonal in the  $SU(3)$  scheme with

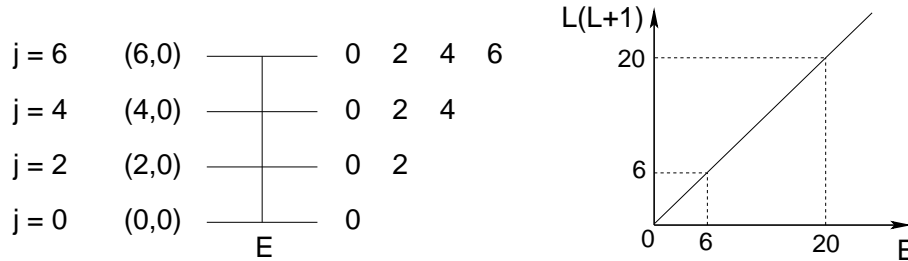


FIGURE 1. Rotational-type spectrum, Elliott rule:  $E \propto L(L + 1)$ .

the same eigenvalue for all states of a representation  $(j_1, j_2)$ . But, if these states are classified by their angular momentum, then the energies for given  $(j_1, j_2)$  follow the rotational sequence  $L(L + 1)$ : we obtain a rotational spectrum (see Fig. 1). We can thus say that the degeneracy is removed by a splitting proportional to  $L(L + 1)$ , as shown in Fig. 1. But, as remarked in the Introduction, the  $J^P$  spectrum of even parity in the  $\pi^+ - p$  hadronic sequence shows a spectrum totally different from that indicated in Fig. 1.

It could be observed that the CAM model of resonances leads apparently to the generation of rotational bands. In fact, a naive model of the resonance in the CAM-plane can be roughly stated as follows: the incoming particle orbits around the obstacle and if  $2\pi R/\lambda = \ell$  ( $R =$  radius of the orbit,  $\lambda =$  wavelength  $= h/p$ ,  $\ell$  integer  $=$  angular momentum), then, by taking the square, one obtains  $E = \ell^2/(2I)$  ( $I$  being the moment of inertia), which yields approximately a rotational spectrum (see Fig. 1). Let us note that the simple geometrical condition used above is equivalent to state that resonances occur at those discrete energies at which the wavelength of the incoming particle is such that nodes of the wavefunction are put at the walls of a well, whose radius  $R$  is fixed; if this condition is satisfied, then nearly stationary waves emerge. If the walls are not completely reflecting, the lifetime of the resonance is finite. In fact, there is a wide phenomenological evidence of rotational bands of resonances in non-relativistic ion collisions [20], where the CAM theory can be applied effectively, and a clear evidence of Regge trajectories can be obtained [21]. In these rotational bands one can plot  $L(L + 1)$  versus  $E$  (see Fig. 1) and obtain a slope given by  $2I$  ( $I$  is the moment of inertia). But, as we have already remarked, this is not the case in the hadronic sequences, and specifically in the  $\pi^+ - p$  elastic resonances, where, in addition, the concept and theory of the relativistic rotator seems to be far from a complete and satisfactory solution.

2.1.3. *Vibrational spectrum generated by the  $\mathfrak{sp}(3, \mathbb{R})$  algebra.* Let us come back to Remark 2 made in Subsection 2.1.2: i.e., the Lie algebras  $\mathfrak{sl}(3, \mathbb{R})$  and  $\mathfrak{su}(3)$  are real forms of the same complex algebra  $A_2$ . In the previous subsection we have seen the role played by  $\mathfrak{su}(3)$  in the three-body problem. On the other hand, in the Introduction we have recalled that several authors [6, 7] suggested that the Lie algebra  $\mathfrak{sl}(3, \mathbb{R})$  should be considered in connection with the rule  $\Delta J = 2$  for the orbital angular excitations. In other words, it seems that both algebras play a relevant role in the study of hadronic sequence spectrum. These arguments prompt to consider as good candidate for describing the spectrum of  $\pi^+ - p$  elastic resonances the smallest Lie algebra containing both subalgebras  $\mathfrak{su}(3)$  and  $\mathfrak{sl}(3, \mathbb{R})$ , that is,

the Lie algebra  $\mathfrak{sp}(3, \mathbb{R})$  associated with the symplectic group  $\mathrm{Sp}(3, \mathbb{R})$ . A  $\mathrm{Sp}(3, \mathbb{R})$  transformation can be regarded as a *general linear canonical transformation of both coordinates and momenta in phase space*. We are thus led to look for a group of transformations of vectors in  $\mathbb{R}^{2n}$  ( $n = 6$ ), whose components are coordinates of positions and momenta. Recalling once again that  $\mathbb{R}^{2n} \equiv \mathbb{C}^n$ , it is natural to explore the properties of the group  $\mathrm{U}(6)$ , acting on the unit sphere  $\mathbb{S}^{2n-1} = \mathrm{U}(n)/\mathrm{U}(n-1)$  ( $n = 6$ ).  $\mathrm{U}(n)$  is the group of matrices in  $\mathrm{GL}(n, \mathbb{C})$  (i.e., the group of the complex  $n \times n$  matrices with non-null determinant), which leave invariant the Hermitian form:  $x_1 \bar{y}_1 + \cdots + x_n \bar{y}_n$  in  $\mathbb{C}^n$ . Now, the field  $\mathbb{C}$  can be replaced with the quaternion field  $\mathbb{H}$  by doubling  $\mathbb{C}$  (i.e., obtaining  $\mathbb{C}^2$ ) to get  $\mathbb{H}$  (recall that the algebras  $\mathbb{R}$ ,  $\mathbb{C} = \mathbb{R}^2$ ,  $\mathbb{H} = \mathbb{C}^2$  are all metric algebras). We are thus led to the group  $\mathrm{U}^{\mathbb{H}}(n)$  ( $n = 3$ ), which leaves invariant the Hermitian form

$$(41) \quad (\boldsymbol{\xi}, \boldsymbol{\eta}) = \xi_1 \bar{\eta}_1 + \cdots + \xi_n \bar{\eta}_n,$$

with  $\boldsymbol{\xi} = (\xi_1, \dots, \xi_n) \in \mathbb{H}^n$ ,  $\boldsymbol{\eta} = (\eta_1, \dots, \eta_n) \in \mathbb{H}^n$ , ( $n = 3$ ). The group  $\mathrm{U}^{\mathbb{H}}(n)$  may be regarded as a group of complex matrices, since any quaternion may be identified with a pair  $(u, v)$  of complex numbers ( $\xi = u + v\mathbf{j}$ ). Let

$$(42a) \quad \xi_1 = x_1 + x_{n+1}\mathbf{j}, \dots, \xi_n = x_n + x_{2n}\mathbf{j},$$

$$(42b) \quad \eta_1 = y_1 + y_{n+1}\mathbf{j}, \dots, \eta_n = y_n + y_{2n}\mathbf{j},$$

then we have

$$(43) \quad \begin{aligned} \xi_1 \bar{\eta}_1 + \cdots + \xi_n \bar{\eta}_n &= [x_1 \bar{y}_1 + \cdots + x_n \bar{y}_n + x_{n+1} \bar{y}_{n+1} + \cdots + x_{2n} \bar{y}_{2n}] \\ &+ [(x_{n+1} y_1 - x_1 y_{n+1}) + \cdots + (x_{2n} y_n - x_n y_{2n})]\mathbf{j}, \end{aligned}$$

since  $\overline{u + v\mathbf{j}} = \bar{u} - v\mathbf{j}$  and  $v\mathbf{j} = \mathbf{j}\bar{v}$ . Therefore each element of the group  $\mathrm{U}^{\mathbb{H}}(n)$  conserves the Hermitian form  $x_1 \bar{y}_1 + \cdots + x_{2n} \bar{y}_{2n}$  and the antisymmetric form  $(x_{n+1} y_1 - x_1 y_{n+1}) + \cdots + (x_{2n} y_n - x_n y_{2n})$ . Reciprocally, if a matrix is unitary and symplectic then, regarded as a transformation of  $\mathbb{H}^n$ , conserves the form  $\xi_1 \bar{\eta}_1 + \cdots + \xi_n \bar{\eta}_n$  [22]. We can thus say that  $\mathrm{U}^{\mathbb{H}}(n)$  is isomorphic to the group  $\mathrm{Sp}(n, \mathbb{C}) \cap \mathrm{U}(2n) \equiv \mathrm{Sp}(n)$  (in our case  $n = 3$ ,  $\mathbb{C}^{2n} = \mathbb{C}^6 = \mathbb{H}^3$ ). Accordingly, the unit sphere  $\mathbb{S}^{4n-1}$  ( $n = 3$ ) may be identified with the space  $\mathrm{Sp}(3)/\mathrm{Sp}(2)$ . Next, taking the intersection  $\mathrm{Sp}(n) \cap \mathrm{O}(2n)$ , one obtains [22]

$$(44) \quad \begin{aligned} \mathrm{Sp}(n) \cap \mathrm{O}(2n) &= \mathrm{Sp}(n, \mathbb{C}) \cap \mathrm{U}(2n) \cap \mathrm{O}(2n) \\ &= \mathrm{Sp}(n, \mathbb{R}) \cap \mathrm{U}(2n) \simeq \mathrm{U}(n), \end{aligned}$$

which implies  $\mathrm{U}(n) \subset \mathrm{Sp}(n, \mathbb{R})$ . The following chain is particularly relevant in our analysis:

$$(45) \quad \mathrm{Sp}(3, \mathbb{R}) \supset \mathrm{U}(3) \supset \mathrm{SU}(3) \supset \mathrm{SO}(3).$$

In Refs. [23, 24] a direct approach is proposed for obtaining the discrete spectrum associated with  $\mathrm{Sp}(3, \mathbb{R})$ , based on the fact that irreducible representations are determined by their highest weight. This amounts to say that two irreducible representations with equal highest weights are equivalent. Furthermore, the representation space is generated by the highest weight vector by the action of the enveloping algebra. Now, the following propositions can be proved.

**Proposition 1** (Ref. [16]). *Every analytic irreducible representation of the real symplectic group  $\mathrm{Sp}(n, \mathbb{R})$  determines and is determined by the highest weight  $m = (m_1, m_2, \dots, m_\nu)$ , whose components are integers satisfying the condition:  $m_1 \geq m_2 \geq \cdots \geq m_\nu \geq 0$ .*

**Proposition 2** (Ref. [23]). *A highest weight state of  $\mathfrak{sp}(3, \mathbb{R})$  is a highest weight vector of its  $\mathfrak{u}(3)$  subalgebra.*

In Ref. [24] the infinitesimal generators of  $\mathfrak{sp}(3, \mathbb{R})$  are constructed by the use of all the Hermitian quadratics in nucleon and momentum coordinates summed over particle index. Next, in order to determine the irreducible unitary representation the authors pass to the quadratics in the harmonic oscillator raising and lowering operators:

$$(46a) \quad b_{ni}^\dagger = \left(\frac{m\omega}{2\hbar}\right)^{1/2} \left(x_{ni} - \frac{i}{m\omega} p_{ni}\right),$$

$$(46b) \quad b_{ni} = \left(\frac{m\omega}{2\hbar}\right)^{1/2} \left(x_{ni} + \frac{i}{m\omega} p_{ni}\right).$$

Thus one obtains a basis of infinitesimal generators of  $\mathfrak{sp}(3, \mathbb{R})$ :

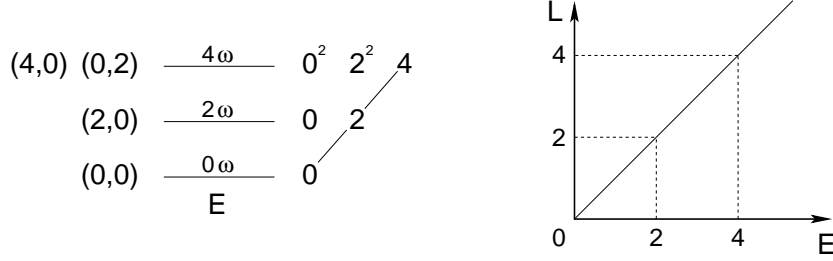
$$(47a) \quad A_{ij} = \sum_n b_{ni}^\dagger b_{nj}^\dagger,$$

$$(47b) \quad C_{ij} = \frac{1}{2} \sum_n (b_{ni}^\dagger b_{nj} + b_{nj} b_{ni}^\dagger),$$

$$(47c) \quad B_{ij} = \sum_n b_{ni} b_{nj}.$$

The  $A_{ij}$  operators are  $2\hbar\omega$  raising operators, the  $B_{ij}$  operators are  $2\hbar\omega$  lowering operators, and the  $C_{ij}$  are  $0\hbar\omega$   $\mathfrak{u}(3)$  operators. Next, it is convenient to represent the  $\mathfrak{su}(3)$  content by the indexes  $\lambda_0 = N_1 - N_2$ ,  $\mu_0 = N_2 - N_3$ , where  $\lambda_0, \mu_0$  are non negative integers with  $N_1 \geq N_2 \geq N_3$ , and  $N_0 = N_1 + N_2 + N_3$  is the harmonic oscillator eigenvalue. Let  $\mathcal{H}_{N_0(\lambda_0, \mu_0)}$  denote the  $\mathfrak{sp}(3, \mathbb{R})$  representation space: it is necessary to decompose this space into subspaces irreducible with respect to the unitary subalgebra  $\mathfrak{u}(3)$ . Let  $\mathcal{H}_{N_0(\lambda_0, \mu_0)}^{(0)}$  denote the subspace containing the highest weight vector, which transforms according to the  $N_0(\lambda_0, \mu_0)$  irreducible representation of  $\mathfrak{u}(3)$ . Since  $A_{ij}$  is a  $2\hbar\omega$  raising operator and  $\mathcal{H}_{N_0(\lambda_0, \mu_0)}$  is spanned by the polynomials in the  $A_{ij}$ 's acting on the  $N_0\hbar\omega$  oscillator space  $\mathcal{H}_{N_0(\lambda_0, \mu_0)}^{(0)}$ , one concludes that the only possible oscillator eigenvalues are  $N_0\hbar\omega, (N_0 + 2)\hbar\omega, (N_0 + 4)\hbar\omega, \dots, (N_0 + 2r)\hbar\omega$  (see [23, Theorem 2.2]). The further reduction of the  $2r\hbar\omega$  eigenspace into irreps of  $\mathfrak{su}(3)$  is accomplished by first expressing the  $r^{\text{th}}$  degree polynomials in the  $A_{ij}$  as  $\mathfrak{su}(3)$  irreducible tensor operators [25] (see also Refs. [26, 27]).

Rosensteel and Rowe work out the problem using the Bargmann–Moshinsky approach [28]. In our present treatment, the  $SU(3)$  representations are labelled by the Cartan indexes  $j_1 = f_2 - f_3 = N_A$  and  $j_2 = f_1 - f_2 = N_B$ ;  $j = j_1 + j_2 = N_A + N_B$ . The Rosensteel–Rowe procedure can be adapted to the present treatment which is close to the Cartan–Dragt presentation. First note that  $j = N_A + N_B$  is the state of highest weight in the sense of Cartan [14]. The Hamiltonian can be written in the following form:  $H = \frac{1}{2}(\mathbf{A}^\dagger \mathbf{A} + \mathbf{A} \mathbf{A}^\dagger + \mathbf{B}^\dagger \mathbf{B} + \mathbf{B} \mathbf{B}^\dagger)$ ; next, one adds the raising operators  $\mathbf{A}^\dagger \mathbf{A}^\dagger$  and  $\mathbf{B}^\dagger \mathbf{B}^\dagger$ , and the lowering operators  $\mathbf{A} \mathbf{A}$  and  $\mathbf{B} \mathbf{B}$ . Starting from the state  $(0, 0)$ , and then applying polynomials of raising operators  $\mathbf{A}^\dagger \mathbf{A}^\dagger$  (or equivalently  $\mathbf{B}^\dagger \mathbf{B}^\dagger$ ) one obtains a spectrum of the harmonic oscillator in a discrete series of the form  $(N_0 + n)\hbar\omega$ , where  $N_0$  is the smallest eigenvalue, and  $n$  is an even

FIGURE 2. Vibrational-type spectrum:  $E \propto L$ .

non-negative integer:  $n = 0, 2, 4, \dots$ . Let us recall that  $\dim(j_1, j_2) = \dim(j_2, j_1)$ . In this way we obtain a vibrational spectrum (i.e.,  $L \propto E$ ), as depicted in Fig. 2.

Since quarks in nucleons move at very nearly the speed of light, we can push forward this non-relativistic model and formulate a conjecture by observing that in relativistic kinematics the connection between the energy  $T$  and the momentum  $p$  is given by  $T^2 = p^2 + m^2$  ( $c = 1$ ), which is the relativistic analog of the relation  $T = p^2/(2m)$ . Then one might expect to have, at the relativistic level,  $L \propto E^2$  (see [10, p. 91]), which corresponds to the actual behavior observed in  $\pi^+$ -p elastic scattering for the first few resonances (see Subsection 3.1).

**2.2. Resonances, echoes and surface waves: from Regge poles to Sommerfeld poles.** The sole possibility of exploring the internal structure of the proton and, in particular, the vibrational spectrum associated with the  $\text{Sp}(3, \mathbb{R})$  group, is to analyze the effects of the interaction of a colliding particle acting as a probe, which hits the proton regarded as a target. A good choice is the  $\pi^+$ -p interaction. Of course this interaction is a two-body problem, and it should be treated with appropriate coordinates in the ambient space  $\mathbb{R}^3$ . On the other hand, all the results concerning the internal structure of the proton have been obtained by the use of the Jacobi coordinates in an ambient space  $\mathbb{R}^6$ . Currently we do not know how to transfer the kinematical and dynamical results obtained in a geometry embedded in  $\mathbb{R}^6$  to a geometry embedded in  $\mathbb{R}^3$ . We are then forced to follow a phenomenological approach and, more specifically, to introduce all what occurs for elaborating a scattering theory which allows us to use the main tools necessary for fitting and interpreting the experimental data, as phase-shifts and cross-sections. From the analysis of these data we can explore the proton structure and, in particular, we can check if the resonances, which eventually appear in the scattering process, correspond to the vibrational spectrum derived in Subsection 2.1.3.

With this in mind, we start from the following integro-differential equation of Schrödinger type:

$$(48) \quad (\Delta + V_D(\mathbf{R}))\chi(\mathbf{R}) + \int_{\mathbb{R}^3} V(\mathbf{R}, \mathbf{R}')\chi(\mathbf{R}') d\mathbf{R}' = E\chi(\mathbf{R}),$$

where  $\Delta$  is the Laplace operator in  $\mathbb{R}^3$ ,  $\mathbf{R}$  is the coordinate of the relative motion between the two interacting particles, and  $\chi(\mathbf{R})$  represents the relative motion wavefunction. In (48) two types of potentials have been introduced: a local one  $V_D(\mathbf{R})$ , and a non-local one  $V(\mathbf{R}, \mathbf{R}')$ , which is here assumed to depend only on the lengths of the vectors  $\mathbf{R}$  and  $\mathbf{R}'$  and on the angle between them;  $E$ , in the case

of the scattering process, represents the scattering relative kinetic energy of the two interacting particles in the c.m.s.. Finally, the constant  $\hbar$  and the reduced mass  $\mu$  do not appear, corresponding to the simple choice of units:  $\hbar = 2\mu = 1$ .

In this treatment we neglect the spin of the proton, the Coulomb potential, and we limit ourselves to consider the non-relativistic scattering of spinless non-identical particles. The need to introduce a non-local potential, in addition to a local one, derives from the fact that beside the phenomenon of resonances also *echoes* are present in the  $\pi^+$ -p elastic scattering: see, in particular, the echo connected with the  $\Delta(\frac{3}{2}, \frac{3}{2})$  resonance (see Subsection 3.1 and Fig. 4). If we describe the scattering process by means of phase-shifts, then an upward crossing through  $\pi/2$  of a phase-shift corresponds to a resonance, whereas a downward crossing through  $\pi/2$  corresponds to an echo. In a neighborhood of an echo, instead of having a *time delay* (proportional to the lifetime of the resonance) we have a *time advance*. In Ref. [20, 29] we have developed a detailed analysis of the resonance-echo process in connection with ion collision. In the present situation the phenomenon is quite similar: when the pion and the proton *get in contact* and successively penetrate each other, the composing quarks come into play. In view of the fermionic character of the quarks and of the Pauli principle, the wavefunction must be antisymmetrized with respect to all particle exchanges. Exchange forces emerge indeed, and these lead to non-local potentials, in close analogy with the ion collision theory [20]. Unfortunately we do not know the precise form of the potentials  $V_D(\mathbf{R})$  and  $V(\mathbf{R}, \mathbf{R}')$ ; therefore we assume only very general properties for these potentials, which allow us to develop a scattering theory and, in particular, to perform a suitable Watson-type resummation of the partial wave expansion, which naturally leads to the introduction of the complex angular momentum (CAM) technique and, specifically, of the Regge poles. In this connection we require that:

- (a)  $V_D(\mathbf{R})$  and  $V(\mathbf{R}, \mathbf{R}')$  are real-valued;  $V(\mathbf{R}, \mathbf{R}')$  is a symmetric function:  $V(\mathbf{R}, \mathbf{R}') = V(\mathbf{R}', \mathbf{R}) = V^*(\mathbf{R}, \mathbf{R}')$ . Accordingly, the Hamiltonian  $H = (-\Delta + \mathcal{U})$ , where

$$(\mathcal{U}\chi)(\mathbf{R}) = V_D(\mathbf{R})\chi(\mathbf{R}) + \int_{\mathbb{R}^3} V(\mathbf{R}, \mathbf{R}')\chi(\mathbf{R}') d\mathbf{R}'$$

is a time-reversal invariant and formally Hermitian operator;

- (b)  $V(\mathbf{R}, \mathbf{R}')$  is a function only of  $R = |\mathbf{R}|$ ,  $R' = |\mathbf{R}'|$  and  $\cos\gamma = (\mathbf{R} \cdot \mathbf{R}')/(RR')$ . Accordingly, the Hamiltonian  $H$  is a rotationally invariant operator;
- (c)  $V_D(\mathbf{R})$  decreases exponentially for  $|\mathbf{R}| \rightarrow +\infty$ ;
- (d)  $V(\mathbf{R}, \mathbf{R}')$  is measurable in  $\mathbb{R}^3 \times \mathbb{R}^3$ , and a constant  $\alpha$  exists such that

$$(49) \quad C^2 = \int_{\mathbb{R}^3} (1 + R^2) e^{2\alpha R} d\mathbf{R} \int_{\mathbb{R}^3} (1 + R'^2) R'^2 e^{2\alpha R'} V^2(\mathbf{R}, \mathbf{R}') d\mathbf{R}' < \infty.$$

If these conditions are satisfied the scattering amplitude  $f(E, \theta)$  (where  $E$  is the relative energy, and  $\theta$  is scattering angle in the c.m.s.) may be expanded in partial waves (see Refs. [20, 29]):

$$(50) \quad f(E, \theta) = \sum_{\ell=0}^{\infty} (2\ell + 1) a_{\ell}(E) P_{\ell}(\cos \theta),$$

where  $\ell$  denotes the relative angular momentum ( $\hbar = 1$ ),  $P_\ell(\cos \theta)$  are the Legendre polynomials, and  $a_\ell$  reads:

$$(51) \quad a_\ell(E) = \frac{e^{2i\delta_\ell} - 1}{2ik},$$

$\delta_\ell$  being the phase-shifts, and  $k$  the momentum in the c.m.s..

Much more delicate is the question concerning the Watson resummation of the partial wave expansion (50). This resummation requires some rather restrictive conditions on the partial scattering amplitudes which, for instance, must admit a unique interpolation in the CAM-plane in the sense of Carlson's theorem [30]. It has been proved that these constraints are satisfied by a rather limited class of potentials, notably by the Yukawian class [30]. It is well-known that this type of resummation splits the scattering amplitude into two terms: a sum over poles of the scattering amplitude in the CAM-plane and a background integral, whose integration path is usually taken to be parallel to the imaginary axis, i.e., from  $-\frac{1}{2} - i\infty$  to  $-\frac{1}{2} + i\infty$ . We note, however, that in the present situation we are working in the physical region of  $\cos \theta$  (i.e.,  $-1 \leq \cos \theta \leq 1$ ), and we are not interested in the asymptotic behavior of the scattering amplitude for large transmitted momentum. Consequently, in the background integral, we are not forced to take a path running along an axis parallel to the imaginary axis of the CAM-plane, but we can rather close the Watson integration path along the border of an appropriate angular sector  $\Lambda$  in the CAM-plane (see Fig. 3). In spite of this relevant advantage we still need the potentials in question to satisfy some additional conditions. In particular, if we expand the non-local potentials  $V(\mathbf{R}, \mathbf{R}')$  in series as follows:

$$(52) \quad V(\mathbf{R}, \mathbf{R}') = \frac{1}{4\pi RR'} \sum_{\ell=0}^{\infty} (2\ell + 1) V_\ell(R, R') P_\ell(\cos \gamma),$$

( $\cos \gamma = (\mathbf{R} \cdot \mathbf{R}') / (RR')$ ), then we have the so-called *partial potentials*  $V_\ell(R, R')$ , which are given by:

$$(53) \quad V_\ell(R, R') = 2\pi RR' \int_{-1}^1 V(R, R', \cos \gamma) P_\ell(\cos \gamma) d(\cos \gamma).$$

Then, we must require the set of these *partial potentials*  $\{V_\ell\}_{\ell=0}^{\infty}$  to admit a unique Carlsonian interpolation  $V(\lambda; R, R')$  ( $\lambda$  denoting the complex angular momentum) in the half-plane  $\mathbb{C}_{(-1/2)}^+ = \{\lambda \in \mathbb{C} : \text{Re } \lambda > -\frac{1}{2}\}$ . Moreover, this interpolation should possess an exponential decrease, for large values of  $|\lambda|$ , of the following form:  $V(\lambda; R, R') \sim e^{-\eta \text{Re } \lambda}$  ( $\eta > 0$ ). If these conditions are satisfied<sup>1</sup>, then we can sum the partial wave expansion following the method of Watson, and therefore transform the series over discrete values of  $\ell$  into an integral encircling the real positive semi-axis of the CAM-plane. Next, we can deform this integration path into a path composed by arcs of circles and two straight lines which delimit an angular sector  $\Lambda$  in the CAM-plane [31] (see Fig. 3). The contributions along the arcs of circles can be proved to vanish, and then one remains with a sum over poles and a background integral, whose path is composed by the two straight lines only.

---

<sup>1</sup>A complete analysis of the conditions needed to perform a Watson-type resummation of the expansion of the partial waves generated by non-local potentials along the lines indicated here, requires very long and detailed mathematical proofs. This work has been published in a mathematical physics journal [31].



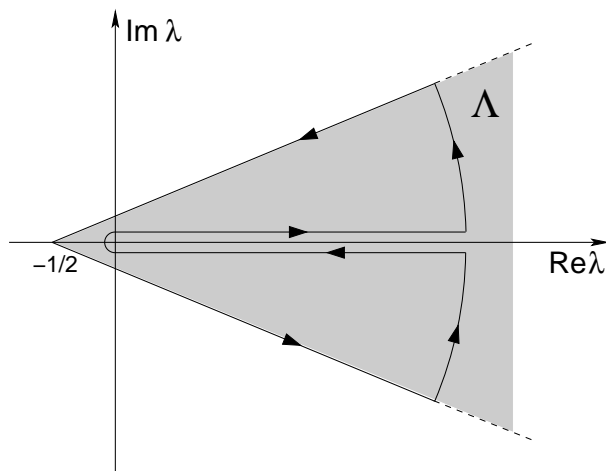


FIGURE 3. The angular sector  $\Lambda$  and the integration path for the computation of the background integral.

We now lay great stress on the following point: *while in the case of local potentials (notably Yukawian) the poles are all located in the first quadrant of the CAM-plane [30], in the case of non-local potentials the poles can lie in both the first and the fourth quadrant of the CAM-plane.* The standard interpretation of the poles lying in the first quadrant associates these singularities to bound states if they are located on the real axis, and to resonances if they lie inside the first quadrant. We can now associate the poles located in the fourth quadrant to the *echoes*. Let us indeed note that these poles are present only in the case of non-local potentials, which are generated by those repulsive forces which emerge when the interacting particles, after getting in contact, penetrate each other. The CAM polology allows us to describe both resonances and echoes by pole singularities: the resonances by poles of the scattering amplitude which lie in the first quadrant; the echoes by poles lying in the fourth quadrant [29]. The imaginary part of the location of the poles lying in the first quadrant is positive (i.e.,  $\text{Im } \lambda > 0$ ) and corresponds to a *time delay*; conversely, the imaginary part of the location of the poles lying in the fourth quadrant is negative (i.e.,  $\text{Im } \lambda < 0$ ), and corresponds to a *time advance*. Let us finally observe that in the classical Breit-Wigner theory the echoes are described by the scattering by an impenetrable sphere. But the roughness of this Breit-Wigner model can be easily verified just observing the behavior of the phase-shifts in several scattering process: for instance, in the elastic  $\alpha$ - $\alpha$  scattering. In this case the phase-shift  $\delta_{(\ell=2)}$ , crossing downward  $\pi/2$  in correspondence of an echo, presents a clearly observable concave behavior [29], instead of a linear one, as prescribed, at sufficiently high energy, by the asymptotic form of the scattering by an impenetrable sphere.

Let us observe that also the type of Watson transformation which we have illustrated above leads to split the total scattering amplitude into a sum over poles plus a background integral. The integration path of this latter term is given by the straight lines which delimit the angular sector  $\Lambda$  in the CAM-plane (see Fig. 3).

The poles can lie either in the first or in the fourth quadrant. In the neighborhood of a resonance one pole, lying in the first quadrant, is dominant, and therefore it is worthwhile to approximate the total scattering amplitude, in the energy domain around a resonance, with the following formula (see also Refs. [21, 29]):

$$(54) \quad f(E, \theta) \simeq g_r(E) \frac{P_{\lambda_r}(-\cos \theta)}{\sin \pi \lambda_r} \quad (0 < \theta \leq \pi),$$

where  $\lambda_r$  gives the location of the pole in the first quadrant (the subscript 'r' is for recalling that we refer to a resonance), and  $P_{\lambda_r}$  is the Legendre function of the first kind. This approximation fails forward (i.e., at  $\theta = 0$  and in a neighborhood of this angle), in view of the cut  $[1, +\infty)$  in the complex  $\cos \theta$ -plane carried by the function  $P_{\lambda_r}(-\cos \theta)$  [11]. We see from formula (54) that if  $|\operatorname{Im} \lambda_r| \ll 1$ , the amplitude  $f(E, \theta)$  presents a pole-type behavior whenever  $\operatorname{Re} \lambda_r$  crosses an integer. Accordingly, a sharp resonance is observed in the cross-section. Amplitude (54) can be projected on the  $\ell^{\text{th}}$  partial wave by means of the following formula [32]:

$$(55) \quad \int_{-1}^{+1} P_\ell(z) P_{\lambda_r}(-z) dz = \frac{2 \sin \pi \lambda_r}{\pi(\lambda_r - \ell)(\lambda_r + \ell + 1)} \quad (\ell = 0, 1, 2, \dots; \lambda_r \in \mathbb{C}),$$

which holds true since  $P_{\lambda_r}(-z)$  presents a singularity of logarithmic type for  $z = 1$  [11]. We thus obtain the following expression for the partial wave scattering amplitude  $a_\ell$ :

$$(56) \quad a_\ell = \frac{e^{2i\delta_\ell} - 1}{2ik} = \frac{g_r}{\pi} \frac{1}{(\alpha_r + i\beta_r - \ell)(\alpha_r + i\beta_r + \ell + 1)},$$

where  $\delta_\ell$  denotes the phase-shift, and  $\lambda_r = \alpha_r + i\beta_r$ . Next, whenever the elastic unitarity condition can be applied, we have the following relationship among  $g_r(E)$ ,  $\alpha_r$ ,  $\beta_r$ :

$$(57) \quad g_r(E) = -\frac{\pi}{k} \beta_r (2\alpha_r + 1) \quad (k^2 = E = \text{energy}),$$

which, finally, yields

$$(58) \quad \delta_\ell = \sin^{-1} \frac{\beta_r(2\alpha_r + 1)}{\left\{ \left[ (\ell - \alpha_r)^2 + \beta_r^2 \right] \left[ (\ell + \alpha_r + 1)^2 + \beta_r^2 \right] \right\}^{1/2}}.$$

When  $\alpha_r(E)$  equals an integer and  $\beta_r(E)$  is very small we have  $\sin \delta_\ell \simeq 1$ , i.e., a resonance. Furthermore, formula (58) can describe a sequence of resonances in various partial waves. Indeed, the pole moves in the CAM-plane as a function of  $E$ , and resonances occur whenever  $\alpha_r(E) = \ell$ ,  $\ell$  integer being the physical angular momentum ( $|\beta_r| \ll 1$ ). We have thus a trajectory which connects several resonances, and, moreover, *the behavior of this trajectory is closely connected with the symmetry properties of the interacting system*, as we have shown in Subsection 2.1. These poles start close to the real positive semi-axis of the CAM-plane (i.e.,  $|\operatorname{Im} \lambda| \ll 1$ ), and constitute the first class of singularities, which correspond to the well-known Regge poles. As the energy  $E$  increases,  $\operatorname{Im} \lambda$  increases too in agreement with the increasing values of the widths of the resonances. Accordingly, the distance of the poles from the real axis of the CAM-plane becomes larger.

In the neighborhood of an echo we can proceed in a way very close to that followed for describing the resonances. Then we write:

$$(59) \quad f(E, \theta) \simeq g_e(E) \frac{P\lambda_e(-\cos\theta)}{\sin\pi\lambda_e} \quad (0 < \theta \leq \pi),$$

where the subscript 'e' stands for recalling that we refer to echoes. Next, projecting the amplitude (59) on the  $\ell^{\text{th}}$  partial wave, we obtain

$$(60) \quad a_\ell = \frac{e^{2i\delta_\ell} - 1}{2ik} = \frac{g_e}{\pi} \frac{1}{(\alpha_e - i\beta_e - \ell)(\alpha_e - i\beta_e + \ell + 1)},$$

where  $\lambda_e = \alpha_e - i\beta_e$  ( $\beta_e > 0$ ). Next, whenever the elastic unitarity condition can be applied, use can be made of the following relationship among  $g_e$ ,  $\alpha_e$ ,  $\beta_e$ :

$$(61) \quad g_e(E) = \frac{\pi}{k} \beta_e (2\alpha_e + 1) \quad (k^2 = E = \text{energy}),$$

which finally yields

$$(62) \quad \delta_\ell = \sin^{-1} \frac{-\beta_e(2\alpha_e + 1)}{\left\{ \left[ (\ell - \alpha_e)^2 + \beta_e^2 \right] \left[ (\ell + \alpha_e + 1)^2 + \beta_e^2 \right] \right\}^{1/2}}.$$

Let us note that, whenever  $\alpha_e$  equals an integer, and  $\beta_e$  is sufficiently small, then  $\delta_\ell \simeq -\pi/2$ . Furthermore, let us remark that resonances and echoes take place at different energies: a resonance occurs at an energy smaller than that of the corresponding echo. Therefore, we may simply sum the two terms representing the resonances and the echoes respectively, and neglect the interference effects. Indeed, at those values of energy where the resonance pole is dominant the term due to the echo is negligible, and vice versa. In conclusion, we can write

$$(63) \quad \begin{aligned} \delta_\ell \simeq & \sin^{-1} \frac{\beta_r(2\alpha_r + 1)}{\left\{ \left[ (\ell - \alpha_r)^2 + \beta_r^2 \right] \left[ (\ell + \alpha_r + 1)^2 + \beta_r^2 \right] \right\}^{1/2}} \\ & + \sin^{-1} \frac{-\beta_e(2\alpha_e + 1)}{\left\{ \left[ (\ell - \alpha_e)^2 + \beta_e^2 \right] \left[ (\ell + \alpha_e + 1)^2 + \beta_e^2 \right] \right\}^{1/2}}. \end{aligned}$$

We can therefore see that both resonances and echoes are described by pole singularities (in the first and in the fourth quadrant of the CAM-plane, respectively), which act at different values of energy, in such a way that their effects can be separated in a rather neat way. Finally, we remark that when the energy increases, the value of  $\beta_e$  increases too; accordingly, approaching the semiclassical limit, the effects of the echoes disappear in agreement with the fact that they are typical *quantum effects*.

As we already said several times, when the energy increases inelastic and reaction channels open, and the target appears as a ball opaque at the center and semitransparent at the border. We have reached the semiclassical limit, and consequently the effects of the echoes can be completely neglected. In order to understand the physical processes connected with the second class of poles, it is convenient and simpler to start from the situation corresponding to the blackbody limit, when the target can be regarded as a totally absorbing opaque ball. In this case the elastic scattering is mainly due to diffraction undergone by the grazing rays. These latter, hitting the target, split into two components: one ray leaves tangentially the diffracting body, and it is called *diffracted ray*, whereas the other ray describes a

geodesic along the border of the ball. The diffracted rays are strongly focused on the horizontal axis, which is a symmetry axis of the body and coincides with the direction of the colliding beam, it is the axial caustic. For what concerns the rays bending the target, we must distinguish between the ones travelling in counterclockwise sense from those travelling in clockwise direction. The scattering angle  $\theta$  must be related to the surface angles  $\theta_m^{(S^+)}$  and  $\theta_m^{(S^-)}$ , where  $\theta_m^{(S^+)}$  refers to the rays winding  $m$  times around the target in counterclockwise sense, and  $\theta_m^{(S^-)}$  refers to the rays winding  $m$  times around the diffracting ball in the clockwise direction. We have:

$$(64a) \quad \theta_m^{(S^+)} = \theta + 2\pi m \quad (m = 0, 1, 2, \dots),$$

$$(64b) \quad \theta_m^{(S^-)} = 2\pi - \theta + 2\pi m \quad (m = 0, 1, 2, \dots).$$

Now, returning to formula (54), we first substitute to  $P_{\lambda_r}(-\cos\theta)$  its asymptotic behavior, which holds for large values of  $|\lambda|$ , i.e., we write (omitting for a while the subscript 'r') [32]:

$$(65) \quad P_{\lambda}(-\cos\theta) \simeq \frac{e^{-i[(\lambda+1/2)(\pi-\theta)-\pi/4]} + e^{i[(\lambda+1/2)(\pi-\theta)-\pi/4]}}{[2\pi(\lambda+1/2)\sin\theta]^{1/2}} \quad (0 < \theta < \pi).$$

Next, we set  $\lambda + \frac{1}{2} = \nu_1$  (the meaning of the subscript '1' in  $\nu_1$  will be clarified below); then we use the following expansion:

$$(66) \quad -\frac{1}{\sin\pi\lambda} = \frac{1}{\cos\pi\nu_1} = 2e^{i\pi\nu_1} \sum_{m=0}^{\infty} (-1)^m e^{i2m\pi\nu_1} \quad (\text{Im } \nu_1 > 0).$$

Finally, from formulae (54), (65), and (66) we obtain, for  $0 < \theta < \pi$ :

$$(67) \quad f(E, \theta) \simeq -iG(E) \sum_{m=0}^{\infty} (-1)^m \left[ \frac{e^{i\nu_1\theta_m^{(S^+)}}}{\sqrt{|\sin\theta_m^{(S^+)}|}} - i \frac{e^{i\nu_1\theta_m^{(S^-)}}}{\sqrt{|\sin\theta_m^{(S^-)}|}} \right],$$

where  $G(E) = 2g(E)e^{-i\pi/4}/\sqrt{2\pi\nu_1}$ . The factor  $(-1)^m$  in (67) is due to the fact that both the counterclockwise and the clockwise rays cross twice the axial caustic at each tour around the diffracting body; since at each crossing there is a phase-shift of  $e^{-i\pi/2}$  for the counterclockwise rays and of  $e^{i\pi/2}$  for the clockwise ones, we have precisely the factor  $e^{\pm i\pi} = -1$ . Furthermore, there is an additional phase-shift between the rays (counterclockwise and clockwise) which explains the factor  $-i = e^{-i\pi/2}$  for the counterclockwise rays and the factor  $i^2 = -1$  for the clockwise ones (see Ref. [33] for a detailed mathematical analysis). The term  $\nu_1$  is given by:  $\nu_1 = \lambda + \frac{1}{2} = R(k + i\gamma_1)$ , where  $R$  is the radius of the diffracting body; accordingly, we have  $kR = \text{Re } \lambda + \frac{1}{2} = \ell + \frac{1}{2}$ , in agreement with the semiclassical expression of the angular momentum. The factor  $\gamma_1$  is due to the damping of the flux of rays travelling along the border of the target, and depends on the curvature of the diffracting body; therefore, it is constant for a spherical ball. The damping is produced by the splitting in two components of each ray bending the target at each point of the target (see also Keller's geometrical theory of diffraction [34]).

Following Sommerfeld [11], the diffraction problem can be treated by starting from Helmholtz's equation and looking for a solution which is continuous throughout the exterior of a given bounded surface  $\Sigma$ , assuming arbitrarily prescribed boundary values on  $\Sigma$ , and a suitable radiation condition at infinity [11]. In the

case of a sphere of radius  $R$  one can separate the variables, the angular part of the solution is expressed in terms of Legendre polynomials, while the radial part is represented by the Hankel functions of the first kind:  $H_{n+1/2}^{(1)}(kr)$  ( $k$  is the wavenumber,  $r$  is the distance from the center of the sphere, and  $n$  is an integer). Sommerfeld imposes a boundary condition of Dirichlet type on the surface of the sphere, i.e.,

$$(68) \quad H_{n+1/2}^{(1)}(kR) = 0.$$

The roots of (68) *lie in the positive imaginary  $n$ -half-plane, and are infinite in number* [11]. To emphasize that the index of these functions acquires complex values, we replace  $n + \frac{1}{2}$  with  $\nu$ , and, accordingly, Eq. (68) will be written  $H_\nu^{(1)}(kR) = 0$ . The roots of the equation  $H_\nu^{(1)}(kR) = 0$  are given, for  $kR \gg 1$ , by the well-known formula obtained by van der Pol and Bremmer with the aid of the Debye expansion for the Bessel function [35]:

$$(69) \quad \nu_m \simeq kR + 6^{-1/3} e^{i\pi/3} (kR)^{1/3} q_m \quad (kR \gg m = 1, 2, 3, \dots),$$

where  $q_m$  is the  $m^{\text{th}}$  zero of the Airy function  $\text{Ai}(q)$ . They are located close to a curve which tends to become parallel to the imaginary axis of the  $\nu$ -plane. In particular, the root of (68) which is closest to the real axis of the  $\nu$ -plane corresponds to the value of  $m = 1$ , and from (69) we have in a first rough approximation  $\text{Re}(\nu_1) \simeq kR$ . In this approach the solution of the diffraction problem can be written in terms of series which, however, converge very slowly. Then Sommerfeld applies a Watson transformation to these series, transforming a sum over  $n$  ( $n$  integer) into an integral along a suitable path in the complex  $\nu$ -plane. The poles of this integral in the  $\nu$ -plane are precisely the roots of the equation  $H_\nu^{(1)}(kR) = 0$ . The sum over residues at the poles located in the first quadrant of the  $\nu$ -plane is rapidly convergent for values of the angle sufficiently large (i.e., backwards). In particular, the term corresponding to the pole closest to the real axis is the dominant one, and it is, in general, sufficient for describing the diffraction in the backward angular region. *This approximation is close to the one we derived from formulae (65) and (67)*, and we return on this point with more details in Subsection 3.2. In particular, the expression of  $\nu_1$ , used in formulae (66) and (67), is given by:  $\nu_1 = \lambda + \frac{1}{2} = R(k + i\gamma_1)$ , and it can be regarded as a crude approximation of the index  $\nu_1$  given by formula (69). Let us finally note that the subscript '1' in the terms  $\nu_1$  and  $\gamma_1$  indicates that we are considering only the pole closest to the real axis.

Now, we return to formula (54), which will be written in the following form:

$$(70) \quad f(E, \cos \theta) \simeq C(E) P_\lambda(-\cos \theta) \quad (0 < \theta \leq \pi),$$

observing that the *elastic unitarity condition cannot be applied* in this context and, moreover, the contribution of  $|\sin \pi \lambda|^{-1}$ , when  $\text{Re} \lambda$  crosses an integral value, is strongly damped by a factor of the form  $\exp(-\pi |\text{Im} \lambda|)$  where, at the blackbody limit,  $|\text{Im} \lambda|$  is of the order of 1. Next we note that the amplitude (70) is indeed factorized into two terms: the first one,  $C(E)$ , gives the amplitude at  $\theta = \pi$  as a function of  $E$  since  $P_\lambda(1) = 1$ ; the second factor describes the backward angular distribution at fixed  $E$ . It follows that two types of phenomenological fits are possible: at fixed angle  $\theta = \pi$ , and at fixed energy (see Subsection 3.2). Let us however note that the scheme of a totally opaque sphere is inadequate at least

for energy ranges below the blackbody limit. We must modify our model assuming that the interaction region presents an absorbing core surrounded by a nearly transparent shell. Therefore, it must be taken into account the contribution to the scattering amplitude also of those grazing rays that undergo limiting refractions, and emerge after taking one or more shortcuts. To this purpose it is worthwhile to mention the important work of Nussenzveig [36], who studied the scattering by a transparent sphere. He uses a Debye expansion, which is a representation of the scattering problem in terms of surface interactions, i.e., the scattering amplitude is decomposed into an infinite series of terms representing the effects of successive internal reflections. In this way Nussenzveig has been able, in particular, to explain the meteorological glory, giving a mathematical and numerical proof of Van De Hulst's conjecture that surface waves are responsible for the meteorological glory: specifically, diffracted rays having taken two shortcuts across the sphere. In a geometrical optics approximation the Debye expansion corresponds to the ray-tracing procedure; using this method, the contributions due to the grazing rays which take  $0, 1, 2, \dots, n$  shortcuts are summed up and, after retaining only the main contribution, the amplitude at backward angles can be written as [37]

$$(71) \quad f(E, \theta) \simeq \sum_{p=0}^n C^{(p)}(E) P_\lambda(-\cos \theta).$$

Since  $P_\lambda(1) = 1$ , from (71) it follows that the interference among the contributions produced by the various components which take shortcuts can explain the oscillations of the cross-section at  $\theta = \pi$ , which are, indeed, present in the  $\pi^+$ -p elastic scattering at energy sufficiently high, as we shall see in Subsection 3.2. As the energy increases the semitransparent corona around the absorbing core gets thinner so that the effects of the shortcuts, and, accordingly, the oscillations of the backward cross-section tend to disappear.

### 3. PHENOMENOLOGICAL ANALYSIS

**3.1. Resonances and echoes.** In the analysis of the  $\pi^+$ -p scattering the spin of the proton must be taken into account. Therefore, we start with a rapid sketch of the main formulae of the scattering amplitude in the case of spin 0-spin  $\frac{1}{2}$  collision. In particular, we have the spin-non-flip amplitude and the spin-flip amplitude, which read, respectively:

$$(72a) \quad f(k, \theta) = \frac{1}{2ik} \sum_{\ell=0}^{\infty} \left[ (\ell+1)(S_\ell^{(+)} - 1) + \ell(S_\ell^{(-)} - 1) \right] P_\ell(\cos \theta),$$

$$(72b) \quad g(k, \theta) = \frac{1}{2k} \sum_{\ell=0}^{\infty} (S_\ell^{(+)} - S_\ell^{(-)}) P_\ell^{(1)}(\cos \theta),$$

where  $k$  is the c.m.s. momentum,  $P_\ell^{(1)}$  is the associated Legendre function, and

$$(73a) \quad S_\ell^{(+)} = \exp(2i\delta_{\ell, \ell+1/2}),$$

$$(73b) \quad S_\ell^{(-)} = \exp(2i\delta_{\ell, \ell-1/2})$$

$\delta_{\ell, \ell \pm 1/2}$  being the phase-shift associated with the partial wave with total angular momentum  $J = \ell \pm \frac{1}{2}$ , where  $\frac{1}{2}$  comes from the proton spin. As a typical example one can keep in mind the  $\Delta(\frac{3}{2}, \frac{3}{2})$  resonance, where the relative angular momentum

of the system is  $\ell = 1$  since the angular momentum of the proton is zero, and taking into account the spin of the proton one has the value  $\frac{3}{2}$  for the total angular momentum; analogously, summing the isotopic spin of the pion with that of the proton one obtains for the total isotopic spin the value  $\frac{3}{2}$ . At higher energies one has to combine the angular momentum of the proton (i.e.,  $L = 2, 4$ ) with the angular momentum carried by the  $P$ -wave pion; finally, taking into account the proton spin one gets the  $J^P$  values of the first three resonances.

The differential cross-section is given by

$$(74) \quad \frac{d\sigma}{d\Omega} = |f|^2 + |g|^2,$$

if the proton target is unpolarized, and if the Coulomb scattering is neglected. Let us indeed note that the Sommerfeld parameter  $\eta = e^2/(\hbar\nu)$  at  $E = 1200$  MeV (close to the energy of the  $\Delta(\frac{3}{2}, \frac{3}{2})$  resonance) is of the order of 0.04. Next, integrating over the angles and taking into account the orthogonality of the spherical harmonics, one obtains for the total cross-section the following expression:

$$(75) \quad \sigma_{\text{tot}} = \frac{2\pi}{k^2} \sum_{J,\ell} (2J+1) \sin^2 \delta_{\ell,J},$$

where  $J = \ell \pm \frac{1}{2}$ . From formula (75) it follows that for the resonance  $\Delta(\frac{3}{2}, \frac{3}{2})$ ,  $\sigma_{\text{tot}} = 8\pi/k^2$ , since  $\sin^2 \delta_{1,3/2} = 1$  at the resonance energy. We can now use a suitably adapted form of (58) for describing the phase-shift  $\delta_{1,3/2}$ , which is responsible of the  $\Delta(\frac{3}{2}, \frac{3}{2})$  resonance. Moreover, the same formula, at different values of  $\ell$ , can reproduce the other phase-shifts  $\delta_{\ell,\ell+1/2}$  ( $\ell = 3, 5$ ), which generate the resonances  $\Delta(\frac{7}{2}, \frac{3}{2})$  and  $\Delta(\frac{11}{2}, \frac{3}{2})$ . Since we interpolate the phase-shifts with odd values of  $\ell$ , the argument of  $\sin^{-1}$  must be multiplied by the factor  $\frac{1-(-1)^\ell}{2}$  which derives from the requirement of antisymmetrization of the scattering amplitude. Therefore, denoting for brevity  $\delta_\ell^{(\pm)} \equiv \delta_{\ell,\ell\pm 1/2}$ , in the *neighborhood of the resonances* we write:

$$(76) \quad \left( \delta_\ell^{(+)} \right)_r = \sin^{-1} \left\{ \frac{1 - (-1)^\ell}{2} \frac{\beta_r(2\alpha_r + 1)}{\left\{ [(\ell - \alpha_r)^2 + (\beta_r)^2] [(\ell + \alpha_r + 1)^2 + (\beta_r)^2] \right\}^{1/2}} \right\},$$

where the subscript 'r' is for recalling and emphasizing that the pole located at  $\lambda_r = \alpha_r + i\beta_r$  refers to resonances and lies in the first quadrant of the CAM-plane. But formula (76) is not sufficient for representing all the features of the experimental data. We must add also the effect of the echo indeed. To this purpose, from formula (62), and taking into account the antisymmetrization induced by the odd values  $\ell$  of the phase-shifts being considered, we have:

$$(77) \quad \left( \delta_\ell^{(+)} \right)_e = \sin^{-1} \left\{ \frac{1 - (-1)^\ell}{2} \frac{-\beta_e(2\alpha_e + 1)}{\left\{ [(\ell - \alpha_e)^2 + (\beta_e)^2] [(\ell + \alpha_e + 1)^2 + (\beta_e)^2] \right\}^{1/2}} \right\},$$

where the subscript 'e' is for recalling that the pole located at  $\lambda_e = \alpha_e - i\beta_e$  ( $\beta_e > 0$ ) lies in the fourth quadrant of the CAM-plane and refers to an echo. Then, adding

the two contributions (76) and (77) we obtain an approximation for the phase-shifts, which is able to reproduce the sequence of both resonances and echoes,

$$(78) \quad \delta_\ell^{(+)} = \left( \delta_\ell^{(+)} \right)_r + \left( \delta_\ell^{(+)} \right)_e .$$

In order to fit the total cross-section over a large interval of energy (up to 2 GeV; see Fig. 4), we must consider also the contribution coming from the resonance  $\Delta(\frac{1}{2}, \frac{3}{2})$  with  $J^P = \frac{1}{2}^-$  and  $E \simeq 1620$  MeV. In view of its negative parity this resonance does not belong to the family of resonances being considered, whose parity is even, and, consequently, we may treat it separately. To this end we can add in formula (75) an expression of the phase-shift associated to the  $\Delta(\frac{1}{2}, \frac{3}{2})$  strictly analogous to formula (76); moreover, the corresponding echo term can be neglected in view of its small effect. Now, returning to formulae (76) and (77), the functions  $\alpha_r$ ,  $\beta_r$ ,  $\alpha_e$ ,  $\beta_e$  can be parameterized as follows (see also Refs. [21, 29]):

$$(79a) \quad \alpha_r = a_0 + a_1(E^2 - E_0^2),$$

$$(79b) \quad \beta_r = b_1(E^2 - E_0^2)^{1/2} + b_2(E^2 - E_0^2),$$

$$(79c) \quad \alpha_e = c_0 + c_1(E^2 - E_0^2),$$

$$(79d) \quad \beta_e = g_0(E^2 - E_0^2) + g_1(E^2 - E_0^2).$$

where  $E$  is the energy in the c.m.s., and  $E_0$  is the rest mass of the  $\pi^+$ -p system. Finally, substituting in formula (75) the values of  $\delta_{\ell,J}$  obtained by formulae (76), (77), (78) and (79), the experimental total cross-section can be fitted. The result is the solid line shown in Fig. 4. From this fit we observe clearly two resonances of even parity, whose  $J^P$  values are  $J^P = \frac{3}{2}^+$ , and  $\frac{7}{2}^+$ . A third resonance of even parity, with  $J^P = \frac{11}{2}^+$ , is not visible but can be extrapolated by computing  $(\delta_{(\ell=5)}^{(+)})_{r,e}$  with the parameters obtained from the analysis of the  $\Delta(\frac{3}{2}, \frac{3}{2})$  and  $\Delta(\frac{7}{2}, \frac{3}{2})$  resonances. The numerical values obtained in this way are summarized in Table 1. Plotting  $J = \alpha_r + 1/2$  ( $\alpha_r \equiv \text{Re } \lambda_r$ ) versus  $s$ , we obtain the straight line displayed in the first inset of Fig. 4. Particularly relevant is the value obtained for  $a_1$ , i.e.,  $a_1 \simeq 1/(\text{GeV})^2$  (see formula (79a)), which gives the slope of the linear trajectory. We thus obtain a *phenomenological evidence of a vibrational-like spectrum generated by the  $\mathfrak{sp}(3, \mathbb{R})$  algebra, as it has been derived, at non-relativistic level, in Subsection 2.1.3*. The second inset of Fig. 4 shows the plot of  $\beta_r \equiv \text{Im } \lambda$  against  $s$  along with the values attained at the three resonances; this behavior correctly describes the phenomenological observation that the width  $\Gamma$  of the resonances increases with the energy (see Table 1 for the numerical values). The dashed line in Fig. 4 displays the fit of the total cross-section computed without the echo terms (see Eqs. (79c and d)), and shows with no ambiguity the necessity of introducing a pole singularity in the fourth quadrant of the CAM-plane, as it has been explained in Subsection 2.2. In the case of the  $\Delta(\frac{3}{2}, \frac{3}{2})$  resonance, where the effect is particularly evident, a naive semiclassical argument can support the interpretation of the distortion of the symmetric bell-shaped peak, which is clearly exhibited by the experimental data, in terms of the composite nature of the interacting particles. If we denote by  $R_{\pi p}$  the distance between the pion and the proton, supposed at rest, then the impulse of the incoming pion in the lab frame is  $p_{\text{lab}}^\pi \sim \sqrt{2}\hbar/R_{\pi p}$ , since  $\ell = 1$ . Now, if we set  $R_{\pi p}$  as the distance at which the two particles “*get in contact*”, which can be thought of the order of the proton radius, then the corresponding  $p_{\text{lab}}^\pi$  yields an estimate of the least pion impulse at which the fermionic nature of



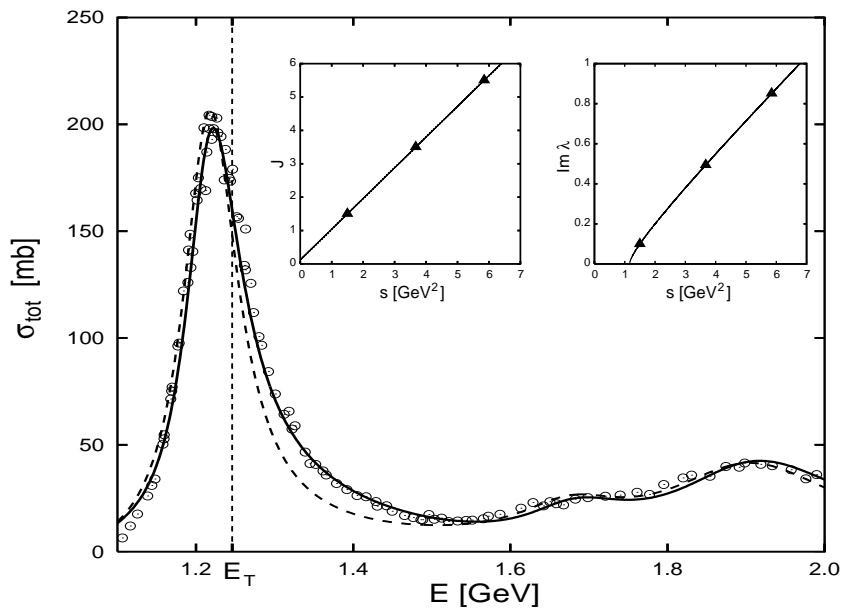


FIGURE 4. Total cross-section. The experimental data (open dots) are taken from Ref. [38], and, for a better visualization, only a subset of the available data have been plotted; for the same reason no error bars are shown. The solid line indicates the total cross-section computed by means of Eq. (75), taking into account the contributions of both the resonance and echo poles generating  $\delta_\ell^{(+)}$  (see formulae (76) and (77)), and the pole associated with the  $\Delta(\frac{1}{2}, \frac{3}{2})$  resonance. The dashed line shows the total cross-section computed by accounting for only the resonance poles (no echo pole). The fitting parameters are (see Eqs. (79)):  $a_0 = 6.89 \times 10^{-1}$ ,  $a_1 = 9.2 \times 10^{-1}(\text{GeV})^{-2}$ ,  $b_1 = 9.0 \times 10^{-2}(\text{GeV})^{-1}$ ,  $b_2 = 1.4 \times 10^{-1}(\text{GeV})^{-2}$ ,  $c_0 = -5.0 \times 10^{-1}$ ,  $c_1 = 5.0 \times 10^{-1}(\text{GeV})^{-2}$ ,  $g_0 = 2.0(\text{GeV})^{-2}$ ,  $g_1 = 3.0(\text{GeV})^{-4}$ . In the left inset  $J \equiv \alpha_r + 1/2$  versus  $s$  is given:  $J = 0.92s + 0.12$ . In the right inset  $\beta_r \equiv \text{Im } \lambda_r$  versus  $s$  is drawn. The triangles indicate the values corresponding to the three resonances with  $J^P = \frac{3}{2}^+, \frac{7}{2}^+, \frac{11}{2}^+$ .

the constituents of the colliding particles enter the picture in the collision process. Then, using  $R_{\pi p} = R_{\text{proton}} \simeq 0.87$  fm we have  $p_{\text{lab}}^\pi \sim 320$  GeV/c, which corresponds to the center of mass energy  $E_T \sim 1246$  MeV, which is indicated in Fig. 4.

**Remark 3.** We have obtained the fits shown in Fig. 4 by using formulae (76) and (77) for the phase-shifts. In these formulae the expression  $[\pm\beta_{r,e}(2\alpha_{r,e} + 1)]$  has been obtained by making use of the unitarity condition (see (61)). This condition holds true only up to a certain value of energy. It is certainly admissible in the energy range including the  $\Delta(\frac{3}{2}, \frac{3}{2})$  resonance, say, up to  $E \sim 1.5$  GeV. Therefore, we can be sure for what concerns the effect of the echo and its explanation by

TABLE 1.  $\pi^+$ -p elastic scattering: Analysis of the resonances. The *purely resonant mass* in the fourth column gives the mass of the resonance computed by means of Eq. (79a) without the contribution coming from the echo pole (see Eq. (79c)). The *purely resonant width*  $\Gamma_R$  indicates the width of the resonance peak computed without the echo contribution, while the *total* width  $\Gamma$  stands for the width of the resonance peak accounting also for the echo term.

$J^P$	Mass [MeV] (present work)	Mass [MeV] (Ref. [38])	Mass [MeV] Resonant	$\Gamma_R$ [MeV] Resonant	$\Gamma$ [MeV] Total	$\Gamma$ [MeV] (Ref. [38])
$\frac{3}{2}^+$	1232.8	1230 – 1233	1224	93	115	116 – 120
$\frac{7}{2}^+$	1951	1915 – 1950	1916	293	308	235 – 335
$\frac{11}{2}^+$	2463	2300 – 2500	2418	397	410	300 – 500

the introduction of a pole in the fourth quadrant of the CAM-plane, as illustrated in Subsection 2.2 and depicted in Fig. 4. But, returning to Fig. 4, we have obtained a good agreement of our fitting formulae with the experimental data up to  $E \sim 2.0$  GeV, in spite of the fact that the unitarity condition is certainly violated for  $1.5 \text{ GeV} \lesssim E \lesssim 2.0 \text{ GeV}$ . For higher values of energy our fits break down as expected. This fact can be tentatively explained conjecturing that our formulae still represent an admissible approximation also beyond the region where the unitarity condition is strictly valid.

**3.2. Surface waves and Sommerfeld poles.** Increasing the energy, at a first cursory examination of the data, a general picture seems to emerge: “*The amplitudes are dominated by diffractive and peripheral contributions*” [2, 3]. For what concerns the resonances Höhler writes [39, pag. S206]: “*If the resonances are ordered according to the shapes of their Argand plots, one finds a continuous transition from textbook-type resonances to tiny wiggles superimposed on a large background.*” Furthermore, Hendry [2] remarks about resonances that: “*The background for a dominant loop tends to be small for energies below the resonance, but grows strongly above the resonance, and quickly swamps it. In terms of diffractive and peripheral picture what is happening is that, as the energy is increased through the resonant region for a particular partial wave, the resonating piece of the partial wave gets buried in a growing diffractive peak.*” Last but not least, at  $p_{\text{cm}} \sim 10 \text{ GeV}/c$  a very large number of partial waves (at least 25) need to be included and this makes the search problem rather cumbersome. In spite of these difficulties and ambiguities, Hendry [2] concludes that there is a good evidence for resonances up to masses of about 4 GeV and spins  $\frac{21}{2}$ . We prefer to follow another approach and investigate up to what extent the diffractive effects can be explained and described by Sommerfeld’s poles.

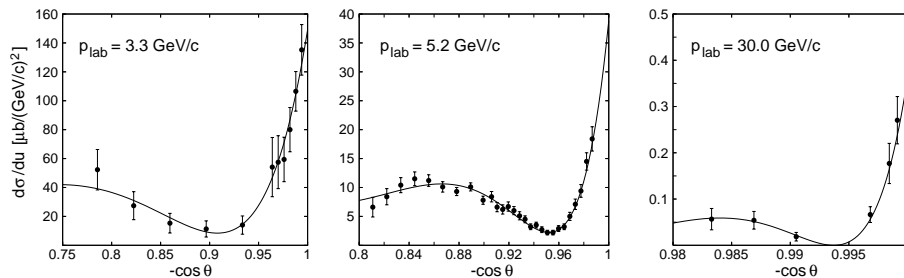


FIGURE 5. Differential cross-section vs.  $(-\cos\theta)$  at  $p_{\text{lab}} = 3.30, 5.20, 30.00$  GeV/c. The solid lines show the differential cross-sections obtained by fitting the experimental data with the function  $(d\sigma/du) = B_0|P_\lambda(-\cos\theta)|^2$ ,  $B_0$  and  $\lambda$  being the fitting parameters. See Table 2 for the summary of the numerical results obtained for momenta ranging in  $2.85$  GeV/c  $\leq p_{\text{lab}} \leq 70$  GeV/c.

We may start from an appropriate extension of formula (70) to account for both the spin-non-flip and the spin-flip amplitudes:

$$(80) \quad \frac{d\sigma}{du} \simeq B_0|P_\lambda(-\cos\theta)|^2 + B_1|P_\lambda^{(1)}(-\cos\theta)|^2,$$

$u$  denoting the appropriate Mandelstam variable. The term  $B_1|P_\lambda^{(1)}(-\cos\theta)|^2$  in formula (80) gives the spin-flip contribution to the differential cross-section. Let us recall, first of all, that formula (80) (as formula (70)) describes the differential cross-section only in the backward direction. Then one notes that by using (80) two types of fits can be performed: (i) at fixed energy; (ii) at fixed angle, i.e.,  $\theta = \pi$ . In Fig. 5 we present fits of the differential cross-section in the backward angular region at various fixed energies. In addition, Table 2 summarizes the numerical results obtained from the analysis of the backward differential cross-section for pion laboratory momenta ranging in the interval  $2.85$  GeV/c  $\leq p_{\text{lab}} \leq 70$  GeV/c. The first observation emerging from these fits is that  $B_1$  (see formula (80)) is negligible compared to  $B_0$ . Then we take  $\text{Re } \lambda \equiv \alpha$ ,  $\text{Im } \lambda \equiv \beta$ , and  $B_0$  as fitting parameters. We are thus able to relate the values of  $\lambda = \alpha + i\beta$  to the location of Sommerfeld's poles: more precisely, to the root of  $H_\nu^{(1)}(kR) = 0$  closest to the real axis (see (69)). Next, we observe that these angular fits are successful if we limit ourselves to consider an extremely backward angular region, whose range has a decreasing spread at increasing energy. A possible explanation of this phenomenology is that, as the energy increases, the distance between two consecutive zeros of  $H_\nu^{(1)}(kR)$  tends to zero, and that the arguments of the zeros tend to  $\pi/2$ , although their real part tends to infinity [35, 45]. Therefore it appears quite reasonable to conjecture that, at increasing energy, the zero of  $H_\nu^{(1)}(kR)$  closest to the real axis is not sufficient anymore to fit the data, but other zeros of  $H_\nu^{(1)}(kR)$  come into play. The values of  $\text{Re } \lambda$  coming from the analysis of the differential cross-section in the backward angular region are displayed in Figs. 6A and B (filled dots) as function of  $p_{\text{cm}}$  ( $p_{\text{cm}} = \hbar k$ ). They clearly appear to lie on a straight line in very good agreement with Sommerfeld's formula (69). This linear behavior is very neat, and is primarily

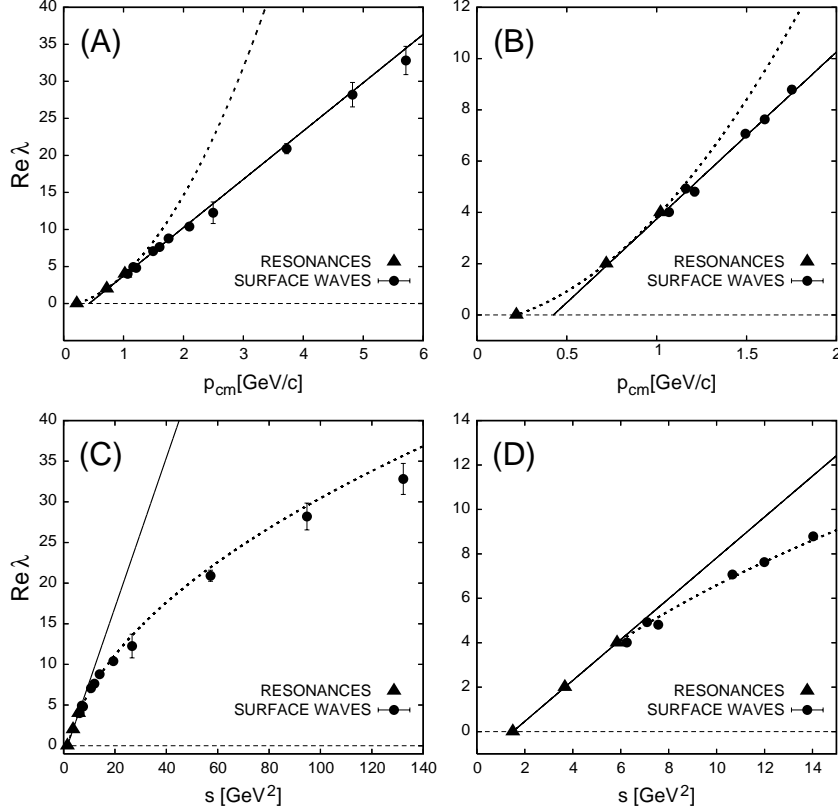


FIGURE 6.  $\text{Re } \lambda$  obtained from the analysis of resonances and surface waves. (A)  $\text{Re } \lambda$  vs.  $p_{\text{cm}}$ . The dots indicate the values of  $\text{Re } \lambda$  obtained from the analysis of the differential cross-section (see text, Table 2, and the legend of Fig. 5). The triangles indicate the values of  $\text{Re } \lambda$  obtained from the analysis of the resonances (see text, Table 1, and the legend of Fig. 4). These values have been lowered by 1 in order to account for the unity pion angular momentum (see Remark 4). The values of  $\text{Re } \lambda$  obtained from the analysis of the differential cross-section have been fitted with a straight line  $\text{Re } \lambda(p_{\text{cm}}) = r_0 (p_{\text{cm}} - p_{\text{cm}}^*)$  (solid line). The fitting parameters are:  $r_0 = 6.52 \pm 0.19 (\text{GeV}/c)^{-1}$ ;  $p_{\text{cm}}^* = (4.3 \pm 0.6) \times 10^{-1} \text{ GeV}/c$ . From the value of the parameter  $r_0$  it results a pion-proton effective interaction radius  $R \sim 1.28 \text{ fm}$  (see Eq. (69)). The dashed line indicates the curve on which the real part of the angular momentum associated with the resonances lie (see Eq. (79a) and the legend of Fig. 4). (B) Zoom of the panel (A) in the momentum range  $0 < p_{\text{cm}} < 2 \text{ GeV}/c$  for better visualization of the transition region. (C)  $\text{Re } \lambda$  vs.  $s$ . As in the previous panels, the triangles denote the values of  $\text{Re } \lambda$  (lowered by 1) associated with the resonances with  $J^P = \frac{3}{2}^+, \frac{7}{2}^+, \frac{11}{2}^+$ . The straight line shows the related Regge trajectory (see Eq. (69) and the legend of Fig. 4). The dashed line shows the fit of the data coming from the analysis of the surface waves (filled dots) with the function  $(d_0 + d_1 \sqrt{s})$ . The fitting parameters are:  $d_0 = -4.45 \pm 0.41$ ;  $d_1 = (3.49 \pm 0.13) (\text{GeV})^{-1}$ . (D) Zoom of the panel (C) in the  $s$ -range  $0 < s < 15 (\text{GeV})^2$ . The dashed line shows the deviation of the real part of the angular momentum associated with the surface waves from the linear Regge trajectory.

TABLE 2.  $\pi^+$ -p elastic scattering: Analysis of the surface waves. Summary of the data resulting from the fits of the differential cross-section at backward angles by means of formula (80) with  $B_1 = 0$ . The angular data, taken from the reference given in the sixth column, have been fitted in the angular range given in the fifth column (see text).

$p_{\text{lab}}$ GeV/c	$B_0$ $\mu\text{b}/(\text{GeV}/c)^2$	Re $\lambda$ —	Im $\lambda$ —	$(-\cos\theta)$ range —	Reference —
2.85	$495.30 \pm 23.01$	$4.01 \pm 0.10$	$0.72 \pm 0.08$	[0.75:1]	[40, 41]
3.30	$149.06 \pm 8.18$	$4.93 \pm 0.16$	$1.00 \pm 0.11$	[0.75:1]	[40, 41]
3.55	$131.91 \pm 7.02$	$4.81 \pm 0.16$	$0.91 \pm 0.12$	[0.75:1]	[40, 41]
5.20	$38.82 \pm 1.88$	$7.07 \pm 0.06$	$1.41 \pm 0.06$	[0.80:1]	[42]
5.91	$36.88 \pm 1.79$	$7.63 \pm 0.09$	$0.53 \pm 0.18$	[0.80:1]	[43]
7.00	$15.93 \pm 1.86$	$8.79 \pm 0.15$	$1.52 \pm 0.19$	[0.85:1]	[42]
9.85	$8.15 \pm 0.79$	$10.40 \pm 0.26$	$1.08 \pm 0.23$	[0.95:1]	[43]
13.73	$3.65 \pm 1.07$	$12.26 \pm 1.46$	$\sim 0.0$	[0.97:1]	[43]
30.00	$(3.62 \pm 0.40) \times 10^{-1}$	$20.91 \pm 0.68$	$1.37 \pm 1.71$	[0.98:1]	[44]
50.00	$(9.48 \pm 1.56) \times 10^{-2}$	$28.20 \pm 1.65$	$3.31 \pm 1.97$	[0.99:1]	[44]
70.00	$(3.41 \pm 0.33) \times 10^{-2}$	$32.82 \pm 1.86$	$4.98 \pm 1.91$	[0.99:1]	[44]

related to the location of the dip in the backward differential cross-section. In Figs. 6C and D the same data are plotted against  $s$  (instead of  $p_{\text{cm}}$ ), and we obtain a square-root dependence, i.e.,  $\text{Re } \lambda \sim \sqrt{s}$ . Moreover, in the same figure, the values of  $\text{Re } \lambda$  associated with the sequence of resonances are also given (filled triangles). From Fig. 6 it emerges clearly that *it is impossible, plotting  $\text{Re } \lambda$  against  $p_{\text{cm}}$  (or, equivalently, against  $s$ ) to locate both the resonances and the surface waves on the same trajectory, i.e., on a single straight line*. In particular, in disagreement with Hendry's analysis, we see that it is impossible to locate the resonances (in particular the  $\Delta(\frac{3}{2}, \frac{3}{2})$  resonance) on a straight line plotting  $\text{Re } \lambda$  versus  $p_{\text{cm}}$  (see Figs. 6A and B). It follows that *resonances and surface waves correspond to two different classes of poles indeed*: the resonances can be described by poles nearly parallel to the real axis of the CAM-plane; the surface waves by poles nearly parallel to the imaginary axis of the CAM-plane. It appears, however, that in the neighborhood of  $p_{\text{cm}} \sim 1.2 \text{ GeV}/c$  a transition occurs between these two classes of poles.

**Remark 4.** In Fig. 6 the values of  $\text{Re } \lambda$  corresponding to the resonances have been lowered by 1, which is precisely the value, in  $\hbar$  units, of the angular momentum of the incoming pion. This subtraction can be justified by observing that in the transition from resonances to surface waves, i.e., from quantum to semiclassical dynamics, the unity angular momentum of the incoming pion smears out in a continuous set of values. Therefore by this artful lowering of 1 ( $\hbar$ ) the connection between resonances and surface waves merges with clear evidence.

In Fig. 7 the plot of  $\text{Im } \lambda \equiv \beta$  versus  $p_{\text{cm}}$  ( $p_{\text{cm}} \equiv \hbar k$ ) is given; Although these data must be taken with care in view of the large errors and of the presence of a few outliers, this figure shows that the values of  $\text{Im } \lambda$  coming from the analysis

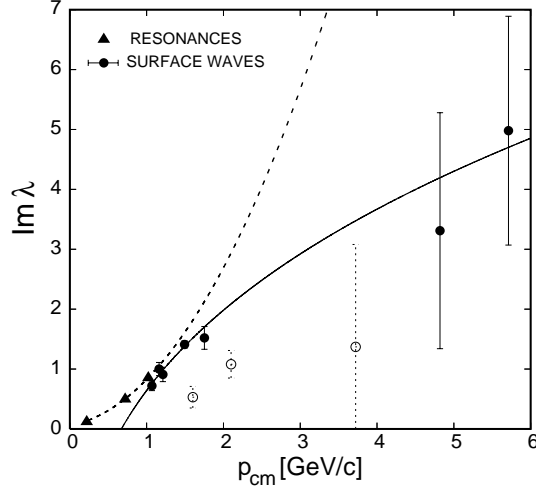


FIGURE 7.  $\text{Im } \lambda$  obtained from the analysis of resonances and surface waves. The dots indicate the values of  $\text{Im } \lambda$  obtained from the analysis of the differential cross-section (see text, Table 2, and the legend of Fig. 5). The triangles indicate the values of  $\text{Im } \lambda$  associated with the resonances (see Eq. (79b) and the legend of Fig. 4). The dashed line displays the fit of the data coming from the analysis of the surface waves with the function  $[h_1(p_{\text{cm}})^{1/3} + h_0]$  (see Eq. (69)). The fitting parameters are:  $h_0 = -4.51 \pm 0.54$ ;  $h_1 = (5.15 \pm 0.49) (\text{GeV}/c)^{-1/3}$ . From the value of  $h_1$  it follows from Eq. (69) the interaction radius  $R \sim 6$  fm. The values of  $\text{Im } \lambda$  resulting from the analysis of the experimental data at  $p_{\text{lab}} = 5.91, 9.85, 13.73$  GeV/c, taken from Ref. [43], and at  $p_{\text{lab}} = 30$  GeV/c from Ref. [44], are shown in ghost form, and have not been included in the fitting procedure.

of the surface waves may belong to a curve whose  $k$ -dependence is of the form  $\beta \sim (kR)^{1/3}$ , in accord with Sommerfeld's pole formula (69). But we must pay a price for this since the value obtained for  $R$  is of the order of 6 fm. Interestingly, as we have seen in Fig. 6, also the behavior of  $\text{Im } \lambda$  indicates a transition between Regge and Sommerfeld poles in a neighborhood of  $p_{\text{cm}} \sim 1.2$  GeV/c (see Fig. 6B).

In Fig. 8 the data of the differential cross-section at  $\theta = \pi$  (see the term  $B_0$  in Eq. (80), and Table 2) are given as function of  $p_{\text{cm}}$ . From a first cursory examination of the data we observe at low  $p_{\text{cm}}$  an anomalous large peak which resembles that encountered in nuclear physics (e.g., in  $\alpha$ - $^{40}\text{Ca}$  elastic scattering) giving rise to the phenomenon called "ALAS" (anomalous large angle scattering). Moreover, an oscillating pattern seems to be superimposed over an inverse power trend (notice the bilogarithmic scale). As the momentum increases the amplitude of the oscillations decreases and tends to zero at large momentum. Also the value of the backward peak is rapidly decreasing for higher values of the center of mass momentum. A first qualitative explanation of these phenomena can be given by following the

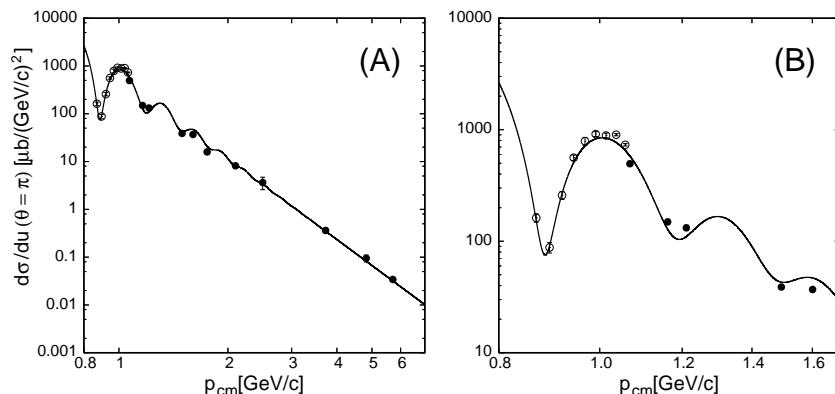


FIGURE 8. Differential cross-section at  $\theta = \pi$  vs. center of mass momentum. (A) The filled dots represent the values of the parameter  $B_0$ , i.e., the differential cross-section extrapolated at  $\theta = \pi$ , obtained from the analysis of the angular distribution (see Fig. 5); the numerical values are summarized in Table 2. The open dots denote the differential cross-section extrapolated at  $\theta = \pi$ , obtained from the analysis of the angular distributions given in Ref. [46]. For the sake of consistency with the analysis performed at higher momenta, the experimental angular data given in Ref. [46] have been fitted with the function  $(d\sigma/du) = B_0 |P_\lambda(-\cos\theta)|^2$  (as in the analysis shown in Fig. 5). However in this case, in view of the limited number of angular data available at each momentum, we used only  $B_0$  as a fitting parameter. At each momentum, we have set  $\text{Re } \lambda(p_{\text{cm}})$  at the value extrapolated from the analysis at higher momenta (see the straight line in Fig. 6A), and  $\text{Im } \lambda = 0$ . These values of differential cross-section at  $\theta = \pi$  differ by a few percent from those given in Ref. [46], which have been extrapolated by using different methods. The solid line represents the fit of the data with the function given in (81); the fitting parameters are:  $p_0 = (3.09 \pm 0.03) \text{ GeV}/c$ ;  $c_1 = -5.61 \pm 0.07$ ;  $c_2 = (-5.55 \pm 1.64) \mu\text{b}/(\text{GeV}/c)^2$ ;  $c_3 = (2.01 \pm 0.33) (\text{GeV}/c)^{-1}$ ;  $\omega = (21.18 \pm 0.04) (\text{GeV}/c)^{-1}$ . (B) Zoom of panel (A) in the range  $0.8 \text{ GeV}/c < p_{\text{cm}} < 1.7 \text{ GeV}/c$  for better visualization of the oscillatory behavior at low momenta.

model presented in Subsection 2.2 (see formula (71)). In the transition region from resonances to surface waves the target appears as an opaque ball at the center surrounded by a semitransparent corona. The hitting rays, which are not absorbed and pass through the corona, focus at backward angles, and produce the anomalous peak. When the momentum increases, the radius of the opaque core increases too, and the backward peak, after some oscillations of decreasing amplitude, diminishes as the semitransparent corona becomes thinner and the blackbody limit is reached. A phenomenological quantitative fit of the data can be performed by means of the

following formula:

$$(81) \quad \left( \frac{d\sigma}{du} \right)_{\theta=\pi} = \left( \frac{p_{\text{cm}}}{p_0} \right)^{c_1} [1 + c_2 e^{-c_3 p_{\text{cm}}} \cos(\omega p_{\text{cm}})],$$

where  $p_0$ ,  $c_i$  ( $i = 1, 2, 3$ ), and  $\omega$  are determined through the fit of the experimental data, and their values are given in the legend of Fig. 8. Formula (81) describes the oscillating decrease of the backward differential cross-section as an inverse power of  $p_{\text{cm}}$  ( $c_1 < 0$ ) with a superimposed oscillating pattern whose amplitude decreases exponentially with the momentum. Let us note that a backward peak in the differential cross-section can also be described by the *baryon exchange mechanism* in the sense of the conventional Regge-pole exchange theory. It is remarkable to note that by the use of this theory one obtains a differential cross-section at  $\theta = \pi$  decreasing as the inverse power of  $p$  with an exponent which is very similar to that obtained by fitting the experimental data with formula (81) [47].

The other relevant feature of the differential cross-section is the forward diffraction peak. But, at  $\theta = 0$ , the function  $P_\lambda(-\cos\theta)$  presents a logarithmic singularity of the following type [11]:

$$(82) \quad P_\lambda(-\cos\theta) \rightarrow \frac{\sin\pi\lambda}{\pi} \log\theta^2,$$

and, consequently, the model elaborated in Subsection 2.2 cannot be used. In the forward scattering the whole sequence of Sommerfeld's poles enter the game since the surface waves describe a small arc of meridian circumference. Furthermore the contribution of the background integral cannot be neglected. One is then led to the ambiguous compensation between two divergent terms: the infinite due to the surface waves at  $\theta = 0$  and the background integral. These two terms should compensate in order to obtain a finite and regular amplitude at  $\theta = 0$ . The resulting amplitude is the forward diffractive peak. However it is out of our purposes to analyze here the scattering in the forward region, which has been studied, as well-known, by using several different methods (for a very recent review on this topic see Ref. [48]). Among the others, one can refer once again to the method based on the *Regge pole exchange*. In view also of these considerations, let us finally remark that our analysis leading to two different classes of poles, Regge's and Sommerfeld's poles in the direct channel, are very well consistent with the standard method of Regge pole exchange.

#### 4. CONCLUSIONS

(1) In agreement with Hendry's analysis we show that in the elastic  $\pi^+ - p$  scattering only the first few resonances, precisely the first three, whose  $J^P$  values are  $J^P = \frac{3}{2}^+, \frac{7}{2}^+, \frac{11}{2}^+$ , lie on a straight line trajectory of a pole in the CAM-plane having the form:  $J^P = \alpha_0 + \alpha' m^2$ ,  $\alpha' \simeq 1/(\text{GeV})^2$ , which is the standard expression of Regge pole trajectory. The conventional picture of linear rising Regge trajectories with universal slope does not hold.

(2) In disagreement with Hendry's analysis we prove that, concerning these first three resonances, it is not possible to obtain a straight line behavior if we plot  $J$  as a function of the center of mass momentum  $k$ .

(3) Beside resonances one must take into account also echoes in order to fit the total cross-section. The advantage of using pole singularities lying in the CAM-plane consists in the possibility of describing the echoes by poles in the fourth quadrant of



- the CAM-plane, instead of introducing the scattering by an impenetrable sphere.
- (4) In agreement with our theoretical analysis, we show that the first three resonances can be associated, in a non-relativistic model, to a vibrational-like spectrum generated by the  $\mathfrak{sp}(3, \mathbb{R})$  algebra.
- (5) At higher energies the amplitudes are dominated by diffractive effects, whose most peculiar features are the creeping waves.
- (6) Resonances and creeping waves cannot be described by the same class of poles. The resonances can be described by a class of poles close to the real positive semi-axis of the CAM-plane: Regge poles. The surface waves can be described by a class of poles lying in the first quadrant of the CAM-plane, which are nearly parallel to the imaginary axis: Sommerfeld's poles.
- (7) At high energy, where the surface waves are dominant, we may fit the differential cross-section at backward angles by the formula  $(d\sigma/du) \simeq B_0 |P_{\alpha+i\beta}(-\cos\theta)|^2$ ,  $\alpha$  and  $\beta$  giving the location of the Sommerfeld pole which is closest to the real axis of the CAM-plane. After the well pronounced peak at  $\theta = \pi$ , there is a dip, whose location is related to  $\alpha \equiv \text{Re } \lambda$ . Plotting  $\alpha$  versus  $k$  we obtain a straight line in good agreement with Sommerfeld's formula which gives  $\text{Re } \lambda + \frac{1}{2} \simeq kR$ .

## REFERENCES

- [1] A.J.G. Hey, R.L. Kelly, Baryon spectroscopy, *Phys. Rep.* 96 (1983) 71–204.
- [2] A.W. Hendry, Pion–nucleon scattering up to 10 GeV/c, *Ann. Phys.* 136 (1981) 1–18.
- [3] A.W. Hendry, Analysis of pion–nucleon scattering up to 10 GeV/c, *Phys. Rev. Lett.* 41 (1978) 222–225.
- [4] V.D. Barger, D.B. Cline, *Phenomenological Theories of High Energy Scattering*, W.A. Benjamin, New York, 1969.
- [5] R.H. Dalitz, *Symmetries and the strong interaction*, in: J.J.J. Kokkedee (Ed.), *The Quark Model*, Benjamin, New York, 1969.
- [6] Y. Dothan, M. Gell–Mann, Y. Ne'eman, Series of hadron energy levels as representations of non–compact groups, *Phys. Lett.* 17 (1965) 148–151.
- [7] Dj. Šijački, The unitary irreducible representations of  $\overline{\text{SL}}(3, R)$ , *J. Math. Phys.* 16 (1975) 298–311.
- [8] Y. Ne'eman, Spinor–type fields with linear, affine and general coordinate transformations, *Ann. Inst. H. Poincaré, Section A* 28 (1978) 369–378.
- [9] J.P. Elliott, *The nuclear shell model and its relation with the nuclear models*, in: *Selected Topics in Nuclear Theory*, I.A.E.A., Vienna, 1963.
- [10] P.D.B. Collins, *An Introduction to Regge Theory and High Energy Physics*, Cambridge Univ. Press, Cambridge, U.K., 1977.
- [11] A. Sommerfeld, *Partial Differential Equations*, Vol. 6, Academic Press, New York, 1964.
- [12] J.M. Richard, The nonrelativistic three–body problem for baryons, *Phys. Rep.* 212 (1992) 1–76 (see also the references quoted therein).
- [13] N.Ja. Vilenkin, A.U. Klimyk, *Representation of Lie Groups and Spherical Functions*, Vol. 1, Kluwer, Dordrecht, 1991.
- [14] A.J. Dragt, Classification of three-particle states according to  $SU_3$ , *J. Math. Phys.* 6 (1965) 533–553.
- [15] Y.A. Simonov, The three–body problem. A complete system of angular functions, *Sov. J. Nucl. Phys.* 3 (1966) 461–466.
- [16] A.O. Barut, R. Raczka, *Theory of Group Representations and Applications*, Polish Scientific Publ., Warszawa, 1977.
- [17] R. Gilmore, *Lie Groups, Lie Algebras and Some of Their Applications*, Wiley, New York, 1974.
- [18] M. Hamermesh, *Group Theory and its Applications to Physical Problems*, Addison–Wesley, Reading, 1962.
- [19] H. Weyl, *The Theory of Groups and Quantum Mechanics*, Dover, New York, 1959.

- [20] E. De Micheli, G.A. Viano, Non-local potentials and rotational bands of resonances in ion collisions, *Eur. Phys. J. A* 10 (2001) 157–169.
- [21] E. De Micheli, G.A. Viano, Unified scheme for describing time delay and time advance in the interpolation of rotational bands of resonances, *Phys. Rev. C* 68 (2003) 064606.
- [22] M.M. Postnikov, *Leçons de Géométrie – Groupes et Algèbres de Lie*, Mir, Moscow, 1982.
- [23] D.J. Rowe, G. Rosensteel, On the algebraic formulation of collective models III. The symplectic shell model of collective motion, *Ann. Phys. (NY)* 126 (1980) 343–370, and references quoted therein.
- [24] P. Park, J. Carvalho, M. Vassanji, D.J. Rowe, G. Rosensteel, The shell-model theory of nuclear rotational states, *Nucl. Phys. A* 414 (1984) 93–112.
- [25] G. Rosensteel, D.J. Rowe, An analytic formula for  $u(3)$ -boson matrix elements, *J. Math. Phys.* 24 (1983) 2461–2463.
- [26] D.J. Rowe, B.G. Wybourne, P.H. Butler, Unitary representations, branching rules and matrix elements for the non-compact symplectic groups, *J. Phys. A: Math. Gen.* 18 (1985) 939–953.
- [27] D.J. Rowe, Microscopic theory of the nuclear collective model, *Rep. Prog. Phys.* 48 (1985) 1419–1480.
- [28] V. Bargmann, M. Moshinsky, Group theory of harmonic oscillators: (I). The Collective Modes, *Nucl. Phys.* 18 (1960) 697–712; *ibid.*, Group theory of harmonic oscillators (II). The integrals of motion for the quadrupole-quadrupole interaction, *Nucl. Phys.* 23 (1961) 177–199.
- [29] E. De Micheli, G.A. Viano, Time delay and time advance in resonance theory, *Nucl. Phys. A* 735 (2004) 515–539.
- [30] V. De Alfaro, T. Regge, *Potential Scattering*, North-Holland, Amsterdam, 1965.
- [31] J. Bros, E. De Micheli, G.A. Viano, Nonlocal potentials and complex angular momentum theory, *Ann. Henri Poincaré* 11 (2010) 659–764.
- [32] A. Erdelyi (Ed.), *Bateman Manuscript Project, Higher Transcendental Functions*, McGraw-Hill, New York, 1953.
- [33] E. De Micheli, G.A. Viano, Geometrical theory of diffracted rays, orbiting and complex rays, *Russ. J. Math. Phys.* 13 (2006) 253–277.
- [34] R.C. Hansen (Ed.), *Geometric Theory of Diffraction*, IEEE, New York, 1981 (see also the references quoted therein).
- [35] J.B. Keller, S.I. Rubinow, M. Goldstein, Zeros of Hankel functions and poles of scattering amplitudes, *J. Math. Phys.* 4 (1963) 829–832.
- [36] H.M. Nussenzveig, High-frequency scattering by a transparent sphere. I. Direct reflection and transmission. *J. Math. Phys.* 10 (1969) 82–124; *ibid.* High-frequency scattering by a transparent sphere. II. Theory of the rainbow and the glory. *J. Math. Phys.* 10 (1969) 125–176.
- [37] G.A. Viano, Nuclear reaction theory of resonances and surface waves, *Il Nuovo Cimento* 104A (1991) 961–993 (see also the references quoted therein).
- [38] W.-M. Yao *et al.* (Particle Data Group), *J. Phys. G* 33 (2006) 1
- [39] G. Höhler, Two-body partial-wave analyses and determination of resonance parameters, in: C.G. Wohl *et al.*, *Review of particle properties*, *Rev. Mod. Phys.* 56 (1984) S1–S299.
- [40] J. Banaigs *et al.*, Experimental evidence for the onset of baryon exchange in pp backward scattering below 3 GeV/c, *Nucl. Phys. B* 8 (1968) 31–44.
- [41] W.F. Baker *et al.*, Elastic backward scattering of pions and kaons, *Nucl. Phys. B* 9 (1969) 249–272.
- [42] W.F. Baker *et al.*, Elastic forward and backward scattering of  $\pi^-$  and  $K^-$ -mesons at 5.2 and 7.0 GeV/c, *Nucl. Phys. B* 25 (1971) 385–410.
- [43] D.P. Owen *et al.*, High-energy elastic scattering of  $\pi^\pm$ ,  $K^-$ , and  $\bar{p}$  on hydrogen at c.m. angles from  $22^\circ$  to  $180^\circ$ , *Phys. Rev.* 181 (1969) 1794–1807.
- [44] W.F. Baker *et al.*, Pion-proton backward elastic scattering between 30 and 90 GeV/c, *Phys. Rev. D* 27 (1983) 1999–2017.
- [45] W. Magnus, L. Kotin, The zeros of the Hankel function as a function of its order, *Numer. Math.* 2 (1960) 228–244.
- [46] A.J. Lennox *et al.*,  $\pi^+p$  backward elastic scattering from 2 to 6 GeV/c, *Phys. Rev. D* 11 (1975) 1777–1795.
- [47] V.A. Lyubimov, Backward scattering of pions by nucleons, *Sov. Phys. Usp.* 20 (1977) 691–702.

- [48] M.M. Block, Hadronic forward scattering: Predictions for the Large Hadron Collider and cosmic rays, *Phys. Rep.* 436 (2006) 71–215.